bioRxiv preprint doi: https://doi.org/10.64898/2026.02.13.705743; this version posted February 15, 2026. The copyright holder for this preprint (which was not certified by peer review) is the author/funder, who has granted bioRxiv a license to display the preprint in perpetuity. It is made available under a CC-BY-NC 4.0 International license.

MANUSCRIPT TITLE

DNA binding converts an inactive RecQ4-family helicase into a dominant-negative DNA repair factor

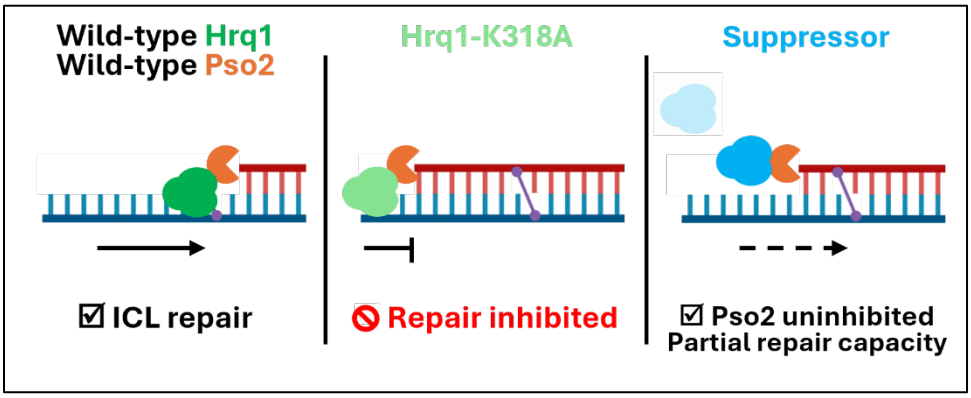
AUTHORS AND AFFILIATIONS

Robert H. Simmons III, Faith E. McDevitt, Alexandra Hurlock, Michael E. Kumcu, and Matthew L. Bochman*

Molecular & Cellular Biochemistry Department, Indiana University, Bloomington, IN 47405, USA

*To whom correspondence should be addressed. Tel: +1 812 856 2095; Email: bochman@iu.edu

GRAPHICAL ABSTRACT



bioRxiv preprint doi: https://doi.org/10.64898/2026.02.13.705743; this version posted February 15, 2026. The copyright holder for this preprint (which was not certified by peer review) is the author/funder, who has granted bioRxiv a license to display the preprint in perpetuity. It is made available under a CC-BY-NC 4.0 International license.

ABSTRACT

DNA inter-strand crosslinks (ICLs) are highly cytotoxic lesions that require coordinated processing to faithfully repair. Members of the RecQ4 helicase family, such as *Saccharomyces cerevisiae* Hrq1, are implicated in ICL repair yet remain poorly understood mechanistically. Hrq1 promotes ICL repair by stimulating the nuclease Pso2, but cells expressing a helicase-dead *hrq1-K318A* allele are more sensitive to ICL damage than *hrq1Δ* cells, indicating a dominant-negative defect. To define the basis of this toxicity, we used unbiased genetic suppressor screening, structural modeling, and biochemical analyses. Spontaneous suppressors of *hrq1-K318A* sensitivity were overwhelmingly intragenic second-site mutations in *hrq1*that either destabilized Hrq1-K318A or disrupted its ability to bind DNA. In all cases, these mutations relieved the dominant-negative repair defect. Biochemical characterization of representative mutants, including a rationally designed DNA-binding mutant, demonstrated that loss of DNA binding abolishes helicase activity and suppresses Hrq1-K318A toxicity despite retaining protein stability. Together, these findings identify persistent DNA binding by a catalytically inactive RecQ4-family helicase as the central driver of dominant-negative ICL repair defects and provide mechanistic insight into how incomplete loss-of-function alleles of human RECQL4 may actively interfere with genome maintenance pathways.

bioRxiv preprint doi: https://doi.org/10.64898/2026.02.13.705743; this version posted February 15, 2026. The copyright holder for this preprint (which was not certified by peer review) is the author/funder, who has granted bioRxiv a license to display the preprint in perpetuity. It is made available under a CC-BY-NC 4.0 International license.

INTRODUCTION

The RecQ family of helicases is an evolutionarily conserved group of enzymes that are found across all domains of life and have well-characterized and important roles in DNA replication, recombination, repair, transcription (1). The human genome encodes five RecQ helicases (RECQL1, WRN, BLM, RECQL4, and RECQL5), four of which cause autosomal recessive genetic diseases when mutated (2-5). These enzymes have also recently emergent targets for cancer therapeutics and diagnostics (1,6). For example, the WRN helicase has been identified as a synthetic lethal target for cancers that display microsatellite instability–high (MSI-H) phenotypes (7-12), while the BLM helicase has gained traction as a drug target to sensitize resistant cancers to alkylating drugs and PARP inhibitors (13-16). Similarly, RECQL4 has entered the spotlight as a tentative druggable target to complement existing cancer therapies (13,17,18).

Despite its established roles in genome integrity and potential status as a prognostic marker for osteosarcoma, breast, and prostate cancers, the physiological functions of RECQL4 remain poorly understood compared to WRN and BLM (13,18-21). This can be partially attributed to the lethality associated with its loss. RECQL4 is an evolutionary chimera, with an N-terminal domain functioning similar to the essential replication initiation factor Sld2 in lower eukaryotes (22) fused to a C-terminal RecQ helicase. Though a majority of its disease-linked and cancer-associated mutations are in the helicase and conserved C-terminal domains (23), RECQL4 helicase activity is not vital to replication (24). However, the *in vivo* study of these alleles remains difficult due to the confounding and potentially lethal pleiotropic effects of perturbing replication initiation. Additionally, RECQL4 is difficult to study biochemically because its large size (135kDa) and long natively disordered N-terminus (first 450 residues) cause it to overexpress poorly with low solubility and a high risk of aggregation in recombinant protein production hosts (25,26). To circumvent these technical limitations and decouple the protein's dual functions, the *Saccharomyces cerevisiae* homolog Hrq1 (27) has emerged as a powerful model system for characterizing the biochemical and genetic functions of human RECQL4.

Extensive foundational work has validated *S. cerevisiae* Hrq1 as a structural and functional homolog of RECQL4 (25,28-37). Both proteins are 3' to 5' helicases containing the conserved RecQ helicase domain but also have degenerate RecQ C-terminal (RQC) and RecQ4 subfamily-specific RHCD (RecQ4/Hrq1-conserved) domains (27). Fibroblasts from patients with Rothmund-Thomson syndrome, an autosomal recessive disease caused by biallelic mutation of *RECQL4*, are sensitized to chemicals that cause DNA inter-strand crosslinks (ICLs) (38), and overexpression of RECQL4 in gastric cancer cells confers resistance to the ICL-inducing agent cisplatin (39). Similarly, *S. cerevisiae* strains lacking Hrq1 (*hrq1Δ*) are sensitive to ICL damaging agents (25,29,30,36,37,40), suggesting the importance of both proteins in ICL repair. Hrq1 functions in a repair pathway with the nuclease Pso2, a homolog of human SNM1A, and both RECQL4 and Hrq1 can specifically stimulate Pso2 nuclease activity *in vitro* (25,29).

Although Hrq1 helicase activity is required for efficient ICL repair, previous work has revealed an intriguing paradox: cells expressing a catalytically inactive *hrq1-K318A* allele are more sensitive to ICL damage than cells lacking *HRQ1* entirely (25,29,30,36). This observation suggests that Hrq1-K318A does

bioRxiv preprint doi: https://doi.org/10.64898/2026.02.13.705743; this version posted February 15, 2026. The copyright holder for this preprint (which was not certified by peer review) is the author/funder, who has granted bioRxiv a license to display the preprint in perpetuity. It is made available under a CC-BY-NC 4.0 International license.

not simply represent a loss-of-function mutation but, instead, interferes with ICL repair in a dominant-negative manner. The mechanistic basis for this interference, however, remains unclear. In particular, it is not known which properties of Hrq1 – DNA binding, protein stability, or interactions with repair partners – are responsible for converting a catalytically inactive helicase into a toxic impediment to repair.

Dominant-negative alleles have long served as powerful tools for dissecting the functional architecture of multiprotein complexes and multistep enzymatic pathways (41-44). In DNA repair systems, dominant-negative proteins can reveal rate-limiting steps, obligate interactions, and vulnerabilities that are not apparent from null mutations alone (45-48). For helicases, dominant-negative effects are often attributed to stable binding to DNA substrates in the absence of productive translocation or remodeling (49-51), yet direct genetic and biochemical evidence for this mechanism remains limited.

Here, we used a combination of genetic suppressor screening, structural modeling, and biochemical analysis to define the basis of *hrq1-K318A*-mediated ICL repair defects. By isolating spontaneous suppressors of *hrq1-K318A* sensitivity to ICL damage, we identified intragenic mutations that alleviate dominant-negative toxicity. Functional characterization of these suppressors revealed that disruption of Hrq1 DNA binding – either through destabilization of the protein or through targeted impairment of DNA interaction – is sufficient to suppress the ICL repair defect caused by catalytic inactivation. These findings clarify the mechanistic role of Hrq1 during ICL repair and provide insight into how DNA engagement by a catalytically inactive RecQ4-family helicase can actively impair genome maintenance pathways.

MATERIALS AND METHODS

Chemical reagents

Diepoxybutane (DEB) was purchased from Sigma-Aldrich (St. Louis, MO, USA), dissolved in anhydrous DMSO to 1 g/mL, and stored at 4°C in the dark. Working concentrations of DEB were produced by further dilution in DMSO or direct dilution into yeast media. ATP was from DOT Scientific (Burton, MI, USA). All other reagents were molecular biology grade or the highest purity available.

Yeast strains

All *S. cerevisiae* strains used in this work (Supplementary Table S1) were derivatives of YPH499 (*MATa ura3-52 lys2-801_amber ade2-101_ochre trp1Δ63 his3Δ200 leu2Δ1*) (52). Genes were deleted as described in (53); the details of strain construction are available upon request. All yeast cells were grown in standard media at 30°C with aeration unless otherwise noted. The yeast expression plasmids used int his work are listed in Supplementary Table S2.

Spot dilution assay

Spot assays were used to compare the sensitivity of wild-type and mutant *S. cerevisiae* strains to the ICL-inducing agent DEB. Generally, 5-mL YPD cultures of indicated strains were incubated overnight at 30°C on a roller drum. Then, the optical density at 600 nm (OD_{600}) of each stain was measured using a

bioRxiv preprint doi: https://doi.org/10.64898/2026.02.13.705743; this version posted February 15, 2026. The copyright holder for this preprint (which was not certified by peer review) is the author/funder, who has granted bioRxiv a license to display the preprint in perpetuity. It is made available under a CC-BY-NC 4.0 International license.

BioPhotometer spectrophotometer (Eppendorf; Hamburg, Germany), and the strains were diluted to an OD_{600} of 1.0 in 100 μL sterile water in a 96-well plate. Each strain was serially diluted tenfold four additional times, and 5 μL of each dilution was then spotted onto a room temperature YPD or YPD + DEB plate in a grid pattern. Plates were grown at 30°C for 2-3 days and imaged with a Bio-Rad (Hercules, CA, USA) ChemiDoc imaging system or a flat-bed scanner. The YPD + DEB plates were made by supplementing freshly autoclaved and slightly cooled (~65°C) YPD medium with DEB to the indicated final concentration, mixing thoroughly, pouring into Petri plates, and curing overnight. Because DEB is highly reactive, the plates were typically used within 24 h. Occasionally, YPD + DEB medium was used 48-72 h after pouring, in which case, it was stored at 4°C prior to use.

Spontaneous suppressor screen

To collect spontaneous suppressors of sensitivity to DEB, 100 μL of OD_{600} = 0.01 *S. cerevisiae* culture was plated onto YPD media containing 250 μg/mL (wild-type), 130 μg/mL (*hrq1Δ*), 70 μg/mL (*hrq1-K318A*), or 50 μg/mL (*pso2Δ*) DEB. After 2 d of growth at 30°C, potential suppressor colonies were identified as colonies growing noticeably better than the background growth visible on the plate. These putative suppressors were restreaked onto YPD plates and YPD containing the same concentration of DEB used initially, with their growth compared to a streak of the parental strain. Any clone displaying better growth than the parental strain on YPD + DEB was then evaluated in a spot dilution assay to semi-quantitatively gauge the level of suppression of DEB sensitivity. Because DEB is a mutagen, reiterative exposure to it during the screening process above would result in the accumulation of mutations at each step. Thus, colonies (that were ultimately proven to be suppressors at the spot dilution stage) from the initial YPD restreak were used for subsequent steps.

Genomic DNA (gDNA) from suppressors was harvested from small YPD overnight cultures using a MasterPure Yeast DNA Purification kit (Lucigen; Middleton, WI, USA), following the manufacturer's instructions. The gDNA was then submitted to the Indiana University Center for Genomics and Bioinformatics (CGB) for small genome sequencing. Libraries were generated with a Nextera Small Genome DNA Library kit and sequenced using a NextSeq instrument (Illumina; San Diego, CA, USA). Bioinformatics support (read mapping and visualization) was also supplied by the CGB.

Amplicon sequencing of the *hrq1-K318A* locus

To sequence just the *hrq1* locus in *hrq1-K318A* suppressor clones, dozens of suppressors were generated and their gDNA was prepared as described above. Then, the locus was amplified by PCR using primers MB527 (5′-GTGAATTGCTCAGAAGAGAAAGGCATACCGTC-3′) and MB528 (5′-CTGTGCATCAACAAGGTGACAGAATGTTGATG-3′) and Bio-Rad iProof HF Master Mix. The DNA was purified using a GeneJet PCR Purification kit (Thermo Fisher Scientific; Waltham, MA, USA), and amplicon sequencing was performed by Plasmidsaurus (Louisville, KY, USA). The suppressor *hrq1* sequences were aligned with the *hrq1-K318A* sequence using CLUSTAL W (54) to identify mutations.

Western blotting

bioRxiv preprint doi: https://doi.org/10.64898/2026.02.13.705743; this version posted February 15, 2026. The copyright holder for this preprint (which was not certified by peer review) is the author/funder, who has granted bioRxiv a license to display the preprint in perpetuity. It is made available under a CC-BY-NC 4.0 International license.

Yeast protein extracts were prepared by adapting the von der Haar hot alkaline lysis procedure (55). Briefly, *S. cerevisiae* strains containing 3xFLAG-tagged wild-type or mutant Hrq1 (Supplementary Table S1) were grown in 5 mL of YPD overnight. The OD_{600} of each strain was measured, and the cultures were diluted to OD_{600} = 0.09 in 50 mL of 30°C YPD grown to an OD_{600} = 1.0. The equivalent of 9 ODs of culture were harvested by centrifugation (4000xg, 5 min) and then resuspended in freshly prepared protein extraction buffer (0.1 M NaOH, 0.05 M EDTA, 2% SDS, and 2% β-mercaptoethanol). The samples were then heated at 95°C for 10 min before being neutralized with 5 µL of 4 M acetic acid. Fifty microliters of loading buffer (250 mM Tris-HCl [pH 6.8], 8% SDS, 40% glycerol, 0.02% Bromophenol Blue, and 200 mM DTT) was added to each sample, and the lysates were then clarified by centrifugation at 14,000 rpm for 5 min in a microcentrifuge. A small aliquot (10 µL) of each sample was loaded onto a 4-15% SDS-PAGE gel and separated at 140 V for 50 min.

After electrophoresis, the gels were removed from their glass plates and gently rinsed with deionized water. Proteins were transferred to nitrocellulose membranes in transfer buffer (25 mM Tris-HCl [pH 8], 192 mM glycine, and 20 mM methanol) at 400 mA for 80 min at 4°C. After transfer, membranes were cut in half at the BLUEstain 2 protein ladder 75 kDa marker (Gold Biotechnology; St. Louis, MO, USA), and each half was blocked in TBS-T (25 mM Tris-HCl [pH 8], 125 mM NaCl, and 0.1% Tween-20) containing 5% (w/v) nonfat dry milk for 30 min at room temperature with gentle rocking. After blocking, the buffer was replaced with fresh TBS-T/5% nonfat dry milk containing a 1:2000 dilution of primary antibody (top half: monoclonal ANTI-FLAG M2-peroxidase antibody [Sigma, A8592]; bottom half: GAPDH loading control antibody [Invitrogen, MA5-15738]) and rocked overnight at 4°C. The next day, membranes were washed five times with 20 mL TBS-T for 5 min each wash. TBS-T containing a 1:15,000 dilution of the secondary antibody (IRDYE 800CW goat anti-mouse IgG secondary antibody, LICORbio; Lincoln, NE, USA) was added to the membranes and rocked at room temperature for 30 min. Then, the membranes were washed as above and briefly washed a final time with deionized water. Membranes were scanned on a LICORbio Odyssey DLx, and Hrq1 and GAPDH protein bands were quantified with Image Studio software.

In silico structural modeling

All structural predictions of Hrq1 were rendered using AlphaFold 3 on the publicly accessible Google DeepMind AlphaFold server (https://alphafoldserver.com/). Structures were rendered with the default parameters, and figures display the overall highest-confidence model. The wild-type Hrq1 protein sequence used for the modeling is from the S288c genotype (https://yeastgenome.org/locus/S000002699), and all Hrq1 mutants were constructed using that template. The *Bacillus subtilis* MrfA structure (56) was retrieved from the protein Data Bank (https://www.rcsb.org/structure/6ZNS). Sequences were visualized in either Chimera X (https://www.cgl.ucsf.edu/chimerax/) or PyMOL (https://www.pymol.org/).

Baculovirus production and insect cell infection

Baculovirus transfer vectors encoding *HRQ1* or mutant *hrq1* genes were constructed as described in (30). Details of plasmid construction are available upon request. Bacmid transfection was performed using

bioRxiv preprint doi: https://doi.org/10.64898/2026.02.13.705743; this version posted February 15, 2026. The copyright holder for this preprint (which was not certified by peer review) is the author/funder, who has granted bioRxiv a license to display the preprint in perpetuity. It is made available under a CC-BY-NC 4.0 International license.

Cellfectin II (Gibco; Waltham, MA, USA) and following the manufacturer's protocol. Briefly, 3 µg of purified bacmid DNA was diluted into 100 µL of Hyclone SFX-insect cell culture medium not containing antibiotics. This dilution was combined with 8 µL of Cellfectin II diluted into 100 µL of the same media, gently flicked to mix, and incubated at room temperature for 15-30 min. During this incubation, $8x10^5$ cells of a low-passage Sf9 insect cell culture were plated onto a 6-well culture plate and left stationary at room temperature for 15 min to allow cells to adhere to the wells. Subsequently, all media was gently aspirated from the wells and replaced with 2 mL of antibiotic-free SFX medium. The roughly 210-µL bacmid-Cellfectin II mixture was then added dropwise to the well. The edges of the 6-well plate were wrapped in a layer of parafilm and incubated at 27°C for 3-5 h. The transfection medium was then aspirated and replaced with 2 mL of SFX medium supplemented with a mix of penicillin, streptomycin, and Amphotericin B (Gibco; Waltham, MA, USA). The plate was again wrapped with parafilm and incubated at 27°C for 4 d. The viral supernatants were harvested from the wells and immediately used for a round of infection.

To amplify the virus further, 20 µL of the viral supernatant harvested from transfection was used to infect $2x10^6$ Sf9 cells in 2 mL of SFX media containing antibiotics in a fresh 6-well plate. This plate was wrapped with parafilm and incubated at 27°C for 4 d. Viral supernatants were harvested from the wells and stored in sterile microcentrifuge tubes at 4°C for up to 2 weeks. Optionally, an additional, identical round of infection can be done with the virus from the first round of infection to further increase the yield of high-titer virus, though this was typically not required. For protein expression, 500 mL Sf9 culture at a density of $1.5x10^6$ cells/mL and >96% live count was infected with 500 µL of high-titer virus (1:1000 dilution)and incubated at 27°C with shaking at 140rpm. Infected cells were harvested after the live count percentage dropped to 70-80% (approximately 48-60 h) by centrifugation at 2000xg for 20 min and stored at -80°C prior to protein purification.

Purification of Hrq1 and Hrq1 mutants

The following protocol was adapted from (28,30). Briefly, frozen pellets from 500 mL infected Sf9 cultures were thawed on ice and resuspended in 200 mL of ice-cold Hrq1 lysis buffer (50 mM Na-HEPES [pH 7.6], 0.4 M NaCl, 20 mM imidazole, and 10% glycerol) supplemented on the same day with protease inhibitor mix (600 nM leupeptin, 2 µM pepstatin A, 2 mM benzamidine, and 1 mM phenylmethanesulfonyl fluoride [PMSF]), 20 µg/ml DNase I, and fresh 5 mM β-mercaptoethanol. The resuspended cell pellet was further lysed via 10 strokes with a Dounce homogenizer on ice. Lysate was clarified by centrifugation at 4°C for 30 min at 14,000 rpm and then loaded onto a lysis buffer-equilibrated gravity column containing 3 mL of HIS-Select Nickel Affinity Gel (Sigma) at 4°C. The resin was washed once with 15 mL lysis buffer containing 5 mM ATP and then twice more with 30 mL of unadulterated lysis buffer. Hrq1-6xHis was eluted using three column volumes of Hrq1 lysis buffer supplemented with 500 mM imidazole. Fractions containing Hrq1 (determined by SDS-PAGE and Coomassie blue staining) were pooled and concentrated to < 1 mL using a 30 kDa MWCO Amicon centrifugal filter at 4°C. The concentrated protein sample was then injected onto a Superdex 200 10/300 GL gel filtration column with a Bio-Rad NGC FPLC system that was pre-equilibrated with Hrq1 storage buffer (25 mM Na-HEPES [pH 8], 30% glycerol, 300 mM NaOAc

bioRxiv preprint doi: https://doi.org/10.64898/2026.02.13.705743; this version posted February 15, 2026. The copyright holder for this preprint (which was not certified by peer review) is the author/funder, who has granted bioRxiv a license to display the preprint in perpetuity. It is made available under a CC-BY-NC 4.0 International license.

[pH 7.6], 25 mM NaCl, 5 mM MgOAc, 1 mM DTT, and 0.1% Tween-20). Hrq1 was eluted with storage buffer at a rate of 0.1 mL/min and collected in 500-µL fractions. Fractions containing Hrq1 were identified using SDS-PAGE and Coomassie blue staining, pooled, and concentrated as above. Concentrated, purified Hrq1 was dispensed into 15-µL aliquots and flash frozen in liquid nitrogen before being stored at -80°C. All Hrq1 mutants were purified identically.

Quantification of recombinant proteins

Our staining procedure was adapted from (57,58). Briefly, a colloidal solution of Coomassie blue G-250 was made by dissolving 100 g of anhydrous ammonium sulfate in 650 mL of deionized water in a 1-L graduated cylinder, stirring until fully dissolved. Then, 100 mL of 200-proof ethanol was added and mixed thoroughly, followed by 200 mg of Coomassie Brilliant Blue G-250 powder, which was stirred until completely dispersed (~20 min). Finally, 10 mL of 85% phosphoric acid was added dropwise while stirring, and then the graduated cylinder was filled to a final volume of 1 L with deionized water. The stain was mixed on a stir plate for ≥ 30 min before use.

Purified proteins were loaded onto 4-15% gradient SDS-PAGE gels alongside BSA standards and were run at 140 V for 50 min. The gels were then removed from their glass plates and soaked in deionized water on a rocker for 30 min. The rinsed gels were placed into clean containers with colloidal Coomassie G-250 stain and rocked for > 2 h. The gels were removed from the stain and quickly rinsed in a clean container several times with deionized water. Then, the gels were rocked in deionized water for > 2 h to destain. Gels were imaged on a Bio-Rad ChemiDoc imaging system, and bands were quantified using ImageJ.

Mass photometry

Mass photometry was used to determine the molecular masses of recombinant proteins and their in-solution oligomerization states, essentially as described (59,60). All analyses were performed on a Refeyn TwoMP system (Oxford, UK) using the accompanying software AcquireMP and DiscoverMP for data acquisition and analysis, respectively. All proteins were diluted to a final concentration of 20 nM in freshly prepared PBS buffer (filtered through a 0.45-µM PES membrane filter and then through a 0.1-µM MCE membrane filter [Millipore; Burlington, MA, USA]). Recordings for each protein were collected over 180 s, and the readings were calibrated with the MassFerence P1 calibration standard (Refeyn) diluted into the same PBS buffer and recorded within 1 h of the other protein measurements.

Electrophoretic mobility-shift assay (EMSA)

EMSAS were performed to measure the DNA binding activity of the purified helicases. Protein was incubated at the indicated concentrations with 1 nM of a single-stranded poly(dT)$_{30}$ oligonucleotide containing a 5′ IRDye700 label (MB1755; 5′-/5IRD700/TTTTTTTTTTTTTTTTTTTTTTTTTTTTTT-3′) for 30 min at 30°C in DNA binding buffer (25 mM Na-HEPES [pH 8.0], 5% glycerol, 50 mM NaOAc [pH 7.6], 150 µM NaCl, 7.5 mM MgOAc, and 0.01% Tween-20). Free single-stranded DNA (ssDNA) was separated from ssDNA-protein complexes on 8% 29:1 acrylamide:bis-acrylamide native-PAGE gels in TG buffer at 100 V

bioRxiv preprint doi: https://doi.org/10.64898/2026.02.13.705743; this version posted February 15, 2026. The copyright holder for this preprint (which was not certified by peer review) is the author/funder, who has granted bioRxiv a license to display the preprint in perpetuity. It is made available under a CC-BY-NC 4.0 International license.

for 50 min at 4°C. Gels were imaged using a LICORbio DLx imager, and bands were quantified with ImageStudio software.

Helicase assays

The DNA unwinding activity of wild-type and mutant Hrq1 was measured using 200 nM of the indicated protein and 1 nM forked DNA substrate. The probe was constructed by incubating 10 μM oligonucleotide MB1772 (5′-/5IRD700/GAACGCTATGTGAGTGACACTTTTTTTTTTTTTTTTTTTTTTT-3′) with 11 μM MB733 (5′-ACCGTTGTGCAACTGAGTGGACAACGTGTCACTCACATAGCGTTC-3′) in a 95°C heat block for 5 min in annealing buffer (20 mM Tris-HCl [pH 8], 4% glycerol, 0.1 mM EDTA, 40 μg/mL BSA, 10 mM DTT, and 10 mM MgOAc). The heat block was then unplugged, and the substrate was allowed to slowly cool to room temperature over 3 h. This created a fork substrate with a 20-bp duplex region, a 25-nt random-sequence 5′-tail, and a 25-nt poly(dT) 3′-tail with nearly 100% efficiency. For the helicase assays, protein was incubated with labelled fork and 100 nM unlabeled MB1772 for 30 min at 30°C in DNA binding buffer containing 2 mM ATP. The reactions were stopped with an equal volume of 2x Proteinase K/SDS stop buffer (20 mM EDTA [pH 8], 1% SDS, 20% glycerol, 0.1% Orange G Dye, and 1 mg/mL Proteinase K). Unwound substrate was separated from annealed substrate, imaged, and quantified as described for the EMSAs above.

Statistical analyses

Data were analyzed and graphed using GraphPad Prism software. The reported values are averages of ≥ 3 independent experiments, and the error bars are the standard deviation. *P*-values were calculated as described in the figure legends, and we defined statistical significance as $p < 0.01$.

bioRxiv preprint doi: https://doi.org/10.64898/2026.02.13.705743; this version posted February 15, 2026. The copyright holder for this preprint (which was not certified by peer review) is the author/funder, who has granted bioRxiv a license to display the preprint in perpetuity. It is made available under a CC-BY-NC 4.0 International license.

RESULTS

S. cerevisiae Fmp48, Tda6, and Ylr297w do not participate in DEB ICL repair

We previously reported that the transcription of three genes of unknown function - *FMP48*, *TDA6*, and *YLR297W* - is significantly upregulated in cells expressing the *hrq1-K318A* allele (34). We hypothesized that perhaps these genes encode proteins involved in DNA ICL repair and that yeast cells upregulated them in the context of a crippled Hrq1-Pso2 ICL repair pathway to compensate for its lack of activity (34,61). In an effort to identify new proteins involved in ICL repair in *S. cerevisiae*, we sought to test that hypothesis here. Individually deleting any of the *FMP48*, *TDA6*, and *YLR297W* genes did not sensitize cells to ICL damage caused by DEB (Fig. 1). However, a role in ICL repair may not be evident when the Hrq1-Pso2 pathway is functional, so we also created double mutants in a *hrq1Δ* background and tested them for ICL sensitivity. There was no synergistic sensitivity to ICL damage above the levels displayed by the *hrq1Δ* single mutant (Fig. 1), suggesting that *FMP48*, *TDA6*, and *YLR297W* likely do not function in the Hrq1-Pso2 ICL repair pathway. Although this is the main repair axis for multiple types of ICL lesions (29,40), a backup proto-Fanconi anaemia (FA) pathway also exists in yeast, which includes enzymes such as the translocase Mph1 and the Chl1 helicase (30). To interrogate the possible involvement of *FMP48*, *TDA6*, and *YLR297W* in the proto-FA pathway, we also created double deletion mutants in a *chl1Δ* strain and tested their ICL sensitivity. As with the Hrq1-Pso2 pathway, no synergistic sensitivity was observed (Fig. 1). Thus, these epistasis analyses suggest that the *FMP48*, *TDA6*, and *YLR297W* gene products do not participate in ICL repair in yeast, at least not of the type of ICL formed by DEB.

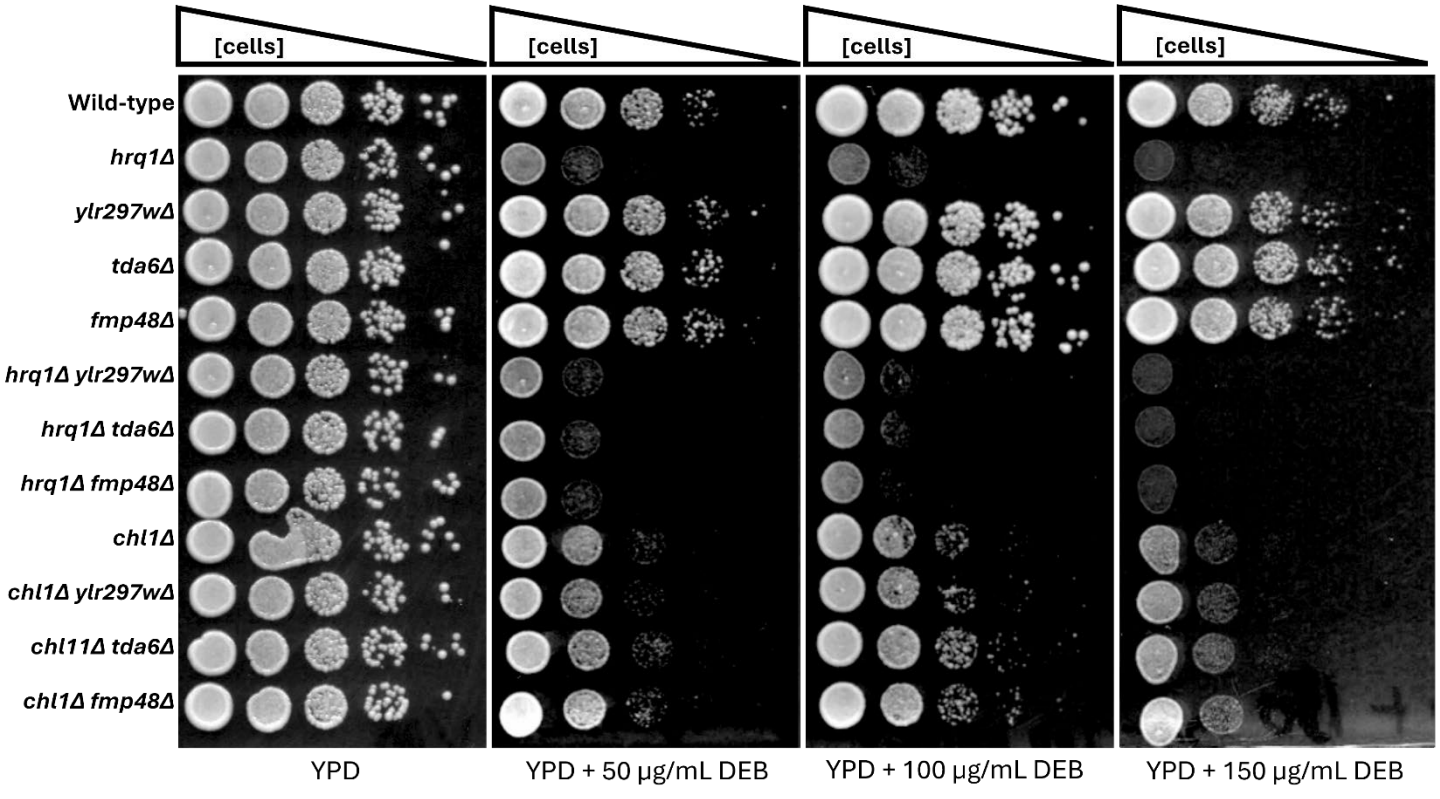


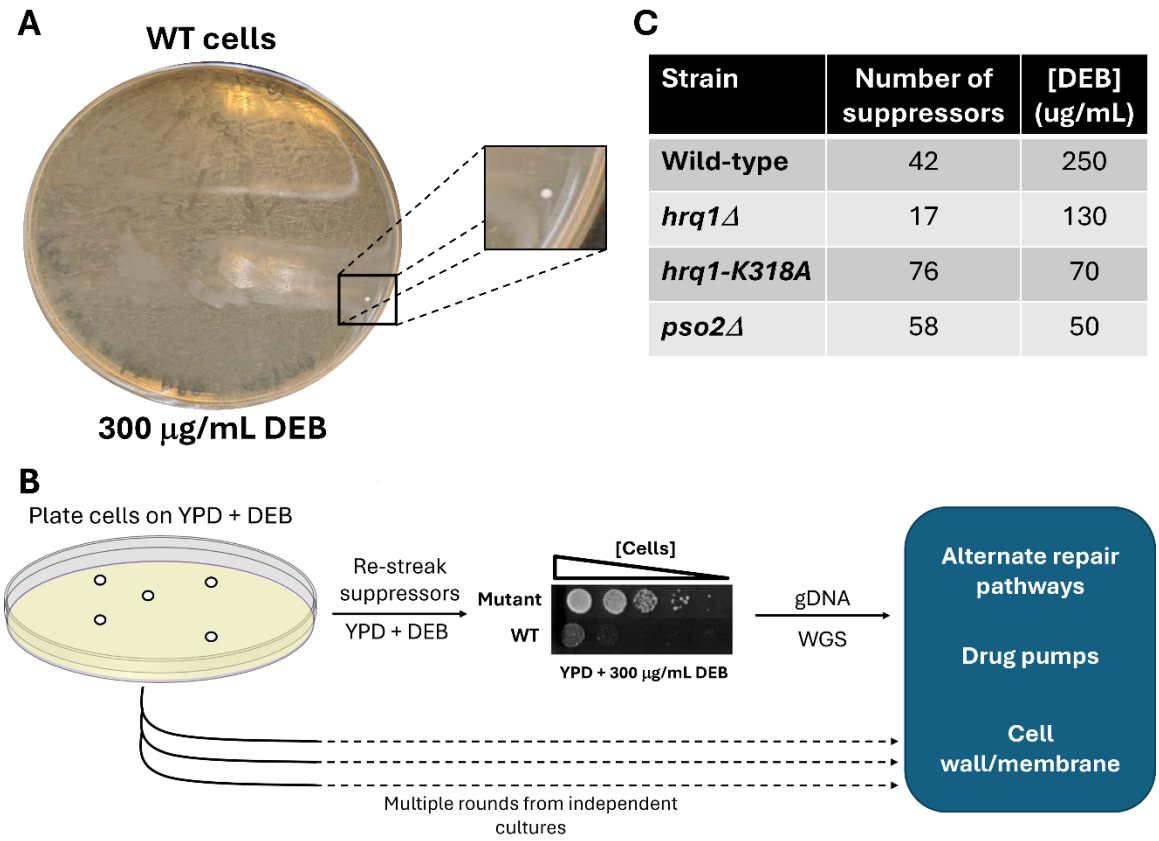
Figure 1. The *FMP48*, *TDA6*, and *YLR297W* genes do not participate in DNA ICL repair in *S. cerevisiae*. Cells of the indicated genotypes were grown in liquid culture, diluted to OD_{600} = 1, and 10-fold serial dilutions were spotted onto plates containing rich medium (YPD) or YPD

bioRxiv preprint doi: https://doi.org/10.64898/2026.02.13.705743; this version posted February 15, 2026. The copyright holder for this preprint (which was not certified by peer review) is the author/funder, who has granted bioRxiv a license to display the preprint in perpetuity. It is made available under a CC-BY-NC 4.0 International license.

supplemented with the indicated concentration of DEB. The plates were then incubated for 2 (YPD and YPD + 50 μg/mL DEB) or 3 (YPD + 100 μg/mL DEB and YPD + 150 μg/mL DEB) days in the dark prior to imaging.

A spontaneous suppressor screen for ICL repair factors

As an alternate method to identify *S. cerevisiae* proteins involved in ICL repair, we performed a spontaneous suppressor screen for mutants displaying resistance to ICL damage. The basis of this screen was the observation that strains exposed to lethal doses of the ICL-inducing agent DEB occasionally yield colonies that are resistant to the DEB concentration used (Fig. 2A). We took advantage of this phenomenon by performing a screen as depicted in Figure 2B. Briefly, *S. cerevisiae* strains were exposed to varying doses of DEB (higher for resistant strains like wild-type, lower for sensitive mutants like *pso2Δ*) on plates, and the suppression in ICL sensitivity of colonies that arose was tested using spot dilution assays on media containing DEB and compared to the parental strain. Genomic DNA was then harvested from verified suppressors and subjected to whole-genome sequencing to identify the genetic source of the resistance to ICL damage. Multiple rounds of the initial plating were used to avoid jackpot mutations (62) that could bias the results. We hypothesized that we would identify mutations that altered the cell wall or cell membranes such that DEB entry into the cells was decreased, mutations in drug pumps that increased their ability to evict DEB from the cells, and mutations that activate or upregulate DNA repair proteins.



Strain	Number of suppressors	[DEB] (ug/mL)
Wild-type	42	250
hrq1Δ	17	130
hrq1-K318A	76	70
pso2Δ	58	50

Figure 2. Screen for suppressors of DEB sensitivity. A) Spontaneous suppressor of DEB sensitivity. WT cells were plated on rich medium containing a lethal dose of DEB, but a single suppressor mutant arose and generated a colony. **B)** Schematic of the suppressor screen. Briefly, suppressors will be collected as in (**A**), restreaked to verify resistance to DEB, compared to the parental strain using spot dilution assays, and then genomic DNA (gDNA) will be harvested for whole-genome sequencing (WGS). Putative pathways affected by suppressor

bioRxiv preprint doi: https://doi.org/10.64898/2026.02.13.705743; this version posted February 15, 2026. The copyright holder for this preprint (which was not certified by peer review) is the author/funder, who has granted bioRxiv a license to display the preprint in perpetuity. It is made available under a CC-BY-NC 4.0 International license.

mutations are shown. **C)** Average number of suppressors *vs.* DEB concentration. The indicated strains were grown, in triplicate, on rich media supplemented with the indicated concentrations of DEB, and the average number of suppressor colonies recovered is reported.

Initially, we performed this screen in *hrq1* and *pso2* mutant backgrounds in an attempt to identify ICL repair factors that can compensate for the loss of the main repair pathway. However, we were also able to gather spontaneous suppressors of ICL sensitivity in wild-type cells in hopes of gaining a more global view of ICL repair. By adjusting the concentration of DEB used to fit the sensitivities of the individual strains analysed, we were able to recover dozens of suppressors per strain (Fig. 2C). Overall, we sequenced the genomes of approximately 8-10 suppressors from wild-type, *hrq1Δ*, and *hrq1-K318A* strains, as well as one pilot suppressor from the *pso2Δ* background (Table 1). The average number of mutations identified per genome roughly scaled with the basal sensitivity of the strains to ICL damage, with the fewest found in WT suppressors and the most in the single *pso2Δ* suppressor. Our initial analyses of these genomics data revealed few common threads, and a technique like bulk segregant analysis (63) will be necessary to identify the genetic cause of suppression for each clone. As that work is ongoing, we instead focus here on suppressors in the *hrq1-K318A* background, which all shared one commonality described below.

Table 1. Whole-genome sequencing results

Strain	No. suppressors screened	Average mutations per genome	Relative sensitivity to DEB*
WT	9	27	+
hrq1Δ	10	67	++
hrq1-K318A	8	85	+++
pso2Δ	1	100	++++

*Relative sensitivity: WT is the least sensitive, and *pso2Δ* is the most sensitive to DEB-induced ICL damage.

Suppressors of *hrq1-K318A* ICL sensitivity are secondary mutations in the helicase

The eight suppressor strains in the *hrq1-K318A* background contained an average of 85 DEB-induced mutations (Table 1), but among them, each strain carried a secondary mutation in the *hrq1-K318A* gene (Fig. 3A). With the exception of the A1006P mutation, which was independently collected twice, all of these second-site mutations were unique, with some causing amino acid substitutions and others introducing frameshifts and/or premature stop codons. To determine if these mutations were responsible for the resistance to DEB, we remade them in the parental *hrq1-K318A* strain, yielding cells with two mutations in *hrq1* in an otherwise wild-type background. In all cases, when plated on medium containing DEB, the double-mutant strains displayed resistance to ICL damage compared to the single *hrq1-K318A* mutant (Fig. 3B, S1, and data not shown). This indicates that the suppression of sensitivity to DEB is a monogenic trait and not due to the cumulative action of multiple mutations in these suppressors. Western blot analysis of several of the full-length mutants confirmed that they are produced *in vivo* (Fig. 3C), though the protein levels of the Hrq1-K318A,C979Y and Hrq1-K318A,A1006P mutants were significantly reduced (p = 0.0036 and 0.0049, respectively) compared to wild-type Hrq1 (Fig. 3D).

It should be noted that cells expressing the *hrq1-K318A* allele are more sensitive to ICL damage than *hrq1Δ* cells (Fig. 3B). This phenotype has been observed before (29,30,64), and we hypothesized that it is due to the *hrq1-K318A* allele being a dominant negative. The protein is expressed at wild-type levels (Fig. 3D), and the model is that it is recruited to its sites of action at ICL damage (29). However, because it is

bioRxiv preprint doi: https://doi.org/10.64898/2026.02.13.705743; this version posted February 15, 2026. The copyright holder for this preprint (which was not certified by peer review) is the author/funder, who has granted bioRxiv a license to display the preprint in perpetuity. It is made available under a CC-BY-NC 4.0 International license.

catalytically inactive, the Hrq1-K318A protein then serves as a roadblock to compensatory repair mechanisms that may be able to repair the lesions. To determine if *hrq1-K318A* is a dominant negative, we cloned *HRQ1* under the control of its native promoter in a single-copy vector, transformed it into *hrq1Δ* and *hrq1-K318A* cells, and then tested sensitivity to DEB relative to cells containing empty vector (Fig. S2). Although *HRQ1* expression was able to rescue the DEB sensitivity of *hrq1Δ* cells, it was much less effective in the *hrq1-K318A* background, supporting the notion that the *hrq1-K318A* allele is dominant negative.

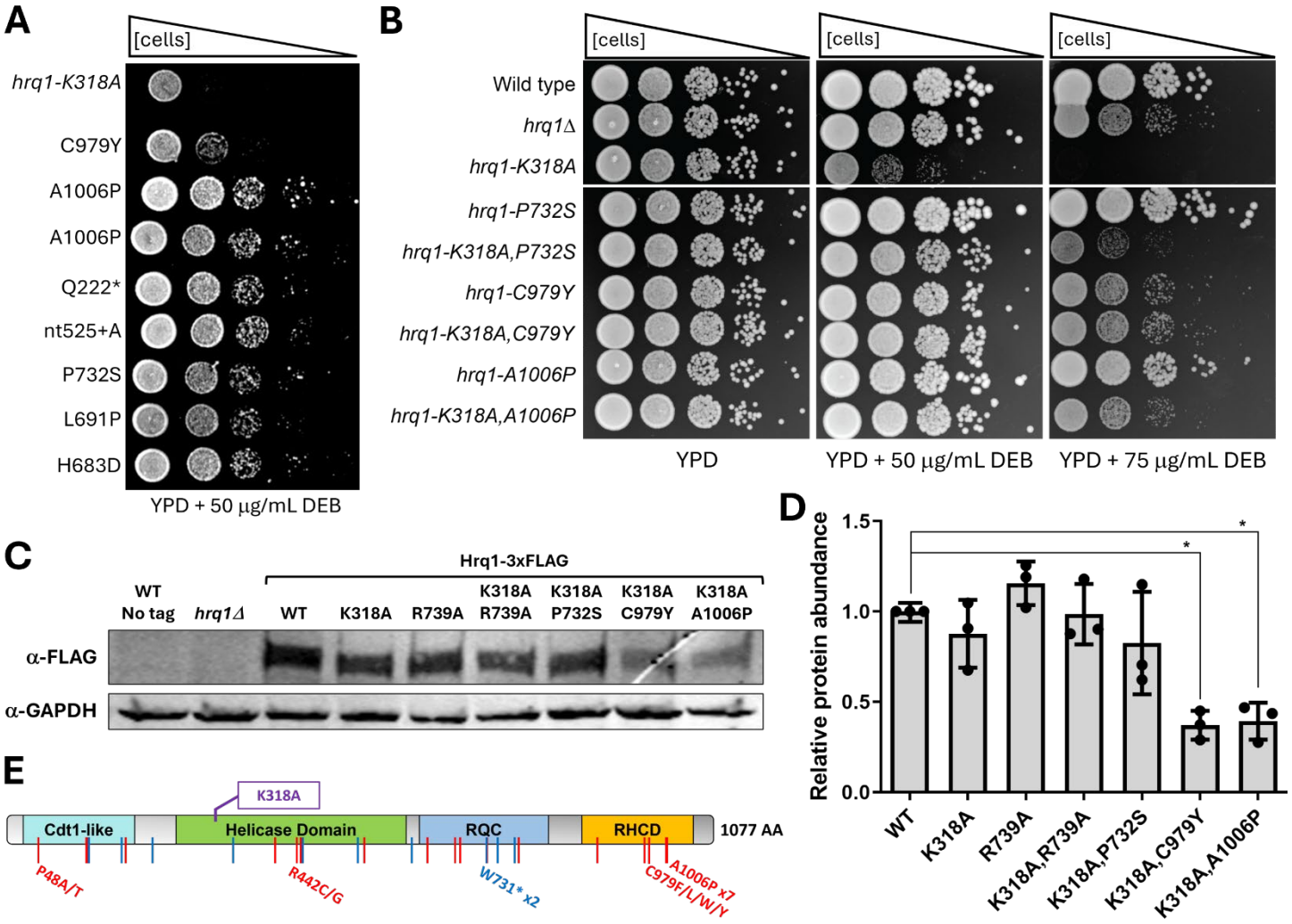


Figure 3. Second-site mutations in *hrq1-K318A* suppress ICL sensitivity. A) Spontaneous suppressor clones from our screen contain secondary mutations in the *hrq1-K318A* locus. Ten-fold serial dilutions of *hrq1-K318A* suppressors containing the mutation listed on the left are shown. The Q222* mutation denotes that Q222 was altered to a stop codon in this strain. The nt525+A mutation denotes the addition of an adenine at nucleotide position 525 in the *hrq1* gene, resulting in a frameshift and early termination in the protein sequence. **B)** Second-site mutations were remade in both wild-type cells the parental *hrq1-K318A* strain, and their sensitivity to DEB was compared to wild-type, *hrq1Δ*, and the *hrq1-K318A* allele alone. **C)** The selected suppressors are produced as full-length proteins *in vivo*. Western blot analysis of protein extracts from the indicated strains. GAPDH protein levels were used as a loading control. **D)** Quantification of n = 3 blots as performed in (C). 3xFLAG-tagged protein abundance was normalized to GAPDH levels in each experiment and then further normalized to wild-type (WT) Hrq1. The amount of Hrq1-K318A,C979Y and Hrq1-K318A,A1006P protein was significantly reduced compared to WT. * $p < 0.01$. **E)** Domain schematic of Hrq1 showing the sites of the suppressor mutants recovered, as well as the location of the K318A mutation. Red hashes denote substitution mutations, and blue lines denote frameshifts/premature stop codons. RQC, RecQ C-terminal domain; RHCD, RecQ4/Hrq1-conserved domain.

bioRxiv preprint doi: https://doi.org/10.64898/2026.02.13.705743; this version posted February 15, 2026. The copyright holder for this preprint (which was not certified by peer review) is the author/funder, who has granted bioRxiv a license to display the preprint in perpetuity. It is made available under a CC-BY-NC 4.0 International license.

Because the suppressor screen performed in the *hrq1-K318A* strain yielded 100% second-site suppressors in the *hrq1-K318A* gene itself, we reasoned that sequencing just the *hrq1* locus in additional suppressors collected in this genetic background would reveal how common this route of suppression is. To do this, we analysed dozens of additional DEB sensitivity suppressors from the *hrq1-K318A* strain collected from the screen depicted in Figure 2B and amplified the *hrq1* locus and flanking regions (~4 kb) for sequencing. From 43 total suppressors, 36 (84%) contained a second-site mutation in the *hrq1-K318A* gene (Table 2). Although mutations at some residues (*e.g.*, P48, R442, W731, C979, and A1006) were recovered more than once, the majority were unique. In some cases, more than one additional mutation was found in the *hrq1-K318A* gene, but such events were less common. Figure 3E shows the sites of these mutations along a domain schematic of Hrq1, revealing no apparent hotspots but, rather, that suppression of DEB sensitivity can result from mutating any of the domains in Hrq1.

Table 2. Hrq1-K318A second-site suppressors

Additional Hrq1-K318A mutations	No. times identified
P48A	1
P48T	1
Q121K, Q125*	1
N122Y	1
nt525+A	1
F181L, V641G	1
Q222*	1
nt1035,1036-GG	1
N409K	1
R442C	1
R442G	1
H448N, Y451*	1
nt1607+T	1
L545F	1
nt1852+A	1
H683D	1
L691P	1
W731*	2
P732S	1
nt2239-G (A747P, V748*)	1
nt2322-C	1
Q780K, S972N	1
A900E	1
C979F	1
C979L	1
C979W	1
C979Y	1
G1005C	1
A1006P	7
None	7

NB: The shading indicates different substitutions at the same residue.

Modelling the mutation sites on Hrq1

Although no mutational hotspots are evident along the primary sequence of Hrq1 (Fig. 3E), as the protein folds into its tertiary structure, distal residues may come into proximity. Unfortunately, no high-resolution structural data exist for Hrq1, so we turned to AlphaFold prediction to determine if any of the suppressor mutations clustered on the protein in three-dimensional space. As shown in Figure 4A, the mutations map to all four domains in the enzyme, with clusters appearing where the helicase domain meets the RQC domain, as well as in the RecQ4/Hrq1-conserved (RHCD) domain. We chose to focus on the latter because the RHCD is only found in RecQ4 family helicases.

Although there is no three-dimensional structure of Hrq1, the crystal structure of the *Bacillus subtilis* homolog, MrfA, was recently solved (56). MrfA lacks the extensive N-terminal domain common to eukaryotic RecQ4 family DNA helicases, but its helicase and C-terminal domains, including the RHCD, display a high level of conservation with *S. cerevisiae* Hrq1 (Fig. S3). This includes a 4-Cys motif that coordinates a Zn^{2+} ion in the MrfA structure (Fig. 4B). In Hrq1, C979 is part of this conserved 4-Cys motif, which has a similar predicted architecture with Zn^{2+} modelled in (Fig. 4C). We isolated four different suppressor mutants at this site (Table 2), and all are predicted to disrupt coordination of a metal ion.

The most commonly collected *hrq1-K318A* suppressor is the A1006P mutation (Table 2), which is located in a portion of Hrq1 not conserved with MrfA (Fig. S3). AlphaFold predicts, with high confidence, that A1006 resides in a short α-helix (K1003-L1014) (Fig. S4). Interestingly, residue A1006 and the α-helix that it is a part of are situated near the 4-Cys motif in the predicted Hrq1 structure (Fig. 4A and S4). An Ala-to-

bioRxiv preprint doi: https://doi.org/10.64898/2026.02.13.705743; this version posted February 15, 2026. The copyright holder for this preprint (which was not certified by peer review) is the author/funder, who has granted bioRxiv a license to display the preprint in perpetuity. It is made available under a CC-BY-NC 4.0 International license.

Pro mutation at residue 1006 would disrupt the N-terminal one-third of α-helix$_{1003\text{-}1014}$ and potentially disrupt the conformation of the protein near the 4-Cys motif.

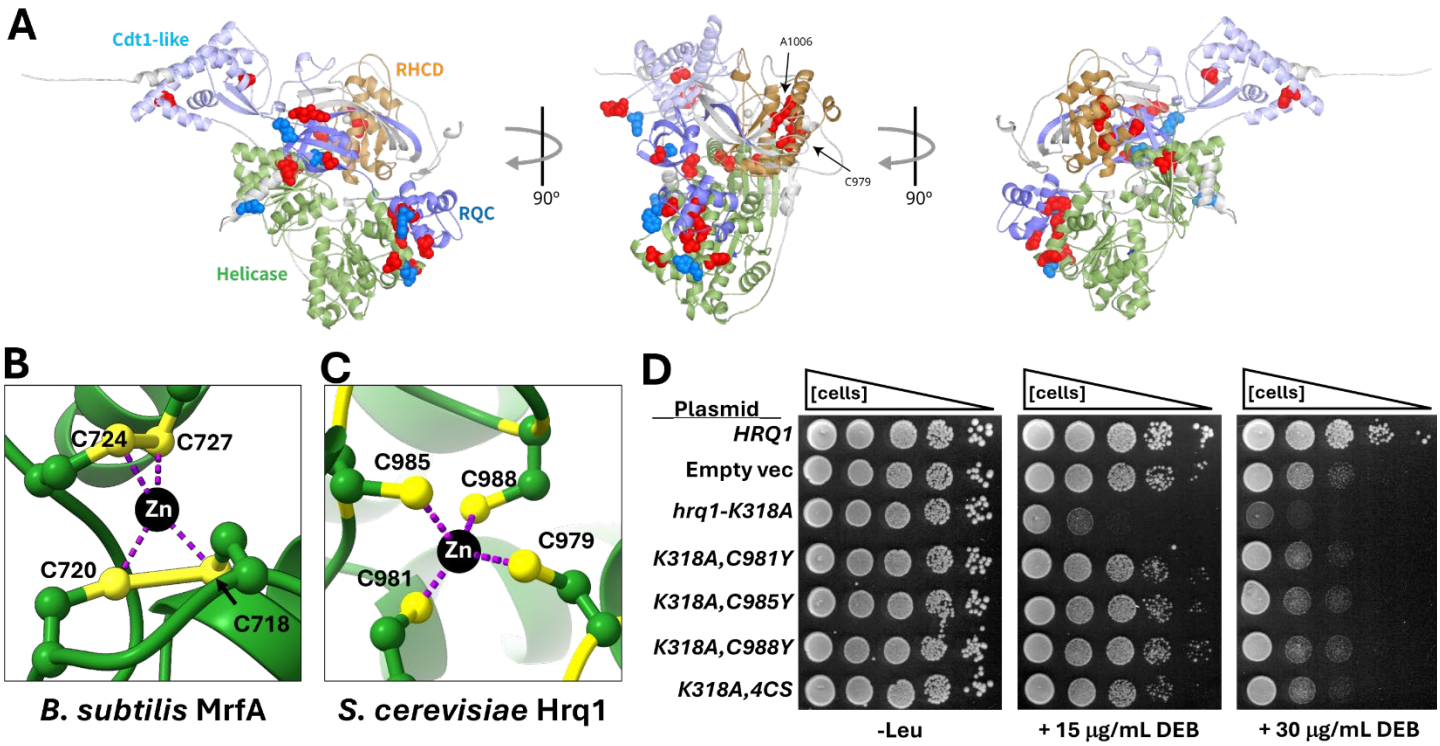


Figure 4. Second-site suppressors map to all Hrq1 domains, including the RHCD. A) Predicted three-dimensional structure of Hrq1 with suppressor mutations mapped. The four domains of the enzyme are marked on the left. Red residues denote substitution mutations, and blue denotes the sites of frameshifts/premature stop codons. The C979 and A1006 sites are labelled in the central panel. **B)** The 4-Cys Zn^{2+} coordination site from the *B. subtilis* MrfA crystal structure (PDB: 6ZNS). **C)** The predicted structure of the 4-Cys motif in *S. cerevisiae* Hrq1 with a Zn ion modelled in. **D)** Mutating any residue in the 4-Cys motif supresses the ICL sensitivity of the *hrq1-K318A* mutant.

Disruption of DNA binding leads to suppression of sensitivity to DEB

Figure 3 shows that the *hrq1-K318A* second-site suppressors that we collected largely phenocopy the DEB sensitivity level of *hrq1Δ* cells. Conceptually, it is simple for a mutant protein to behave like a null. For instance, an unstable helicase that is quickly degraded, lacks nuclear localization, or fails to bind DNA would phenocopy *hrq1Δ* rather than *hrq1-K318A*. Indeed, western blotting indicated that the K318A,C979Y and K318A,A1006P suppressor protein levels are significantly reduced relative to wild-type and Hrq1-K318A alone (Fig. 3C and 3D).

This is an unsurprising result for the C979Y substitution because mutation of the homologous $CXCX_3CX_2C$ motif in the *Mycobacterium smegmatis* homolog of Hrq1, the SftH helicase, also destabilizes the protein (65). To further probe the Hrq1 4-Cys motif, we individually mutated the other three Cys residues (C981, C985, and C988) to Tyr in the context of the Hrq1-K318A protein to mimic Hrq1-K318A,C979Y. These mutants were cloned into a *LEU2*-marked vector under the control of the *HRQ1* promoter and expressed in *hrq1Δ* cells. As shown in Figure 4D, expressing wild-type Hrq1 with this system rescued the DEB sensitivity of the *hrq1Δ* strain, but Hrq1-K318A expression further sensitized the

bioRxiv preprint doi: https://doi.org/10.64898/2026.02.13.705743; this version posted February 15, 2026. The copyright holder for this preprint (which was not certified by peer review) is the author/funder, who has granted bioRxiv a license to display the preprint in perpetuity. It is made available under a CC-BY-NC 4.0 International license.

cells. However, expressing Hrq1-K318A,C981Y, -K318A,C985Y, or -K318A,C988Y phenocopied *hrq1Δ*, as we demonstrated for Hrq1-K318A,C979Y above (Fig. 3B). More conservative Cys-to-Ser mutations were used to examine the 4-Cys motif in *M. smegmatis* SftH, so we also tested a 4xCys-to-Ser Hrq1-K318A mutant (Hrq1-K318A,4CS). Much like the single Cys-to-Tyr mutants, cells expressing Hrq1-K318A,4CS displayed DEB sensitivity like *hrq1Δ* rather than *hrq1-K318A* (Fig. 4D). Thus, mutating any or all of the residues involved in the predicted zinc coordination site suppresses the DEB sensitivity of the *hrq1-K318A* mutation, likely by destabilizing the mutant protein.

Unlike the K318A,C979Y and K318A,A1006P suppressors, the K318A,P732S mutant is expressed at approximately wild-type levels *in vivo* (Fig. 3C and 3D), arguing against protein instability as the only route to the suppression of ICL sensitivity. The nuclear localization sequence (NLS) of Hrq1 has not been identified, but cNLS Mapper (66) predicts that it exists from amino acids 932-942 (ERQTKRKRPAR). This motif is not impacted by any of the suppressor mutations that we isolated, other than those with frameshifts and/or early stop codons (Table 2). However, even if the predicted NLS is wrong, lack of nuclear localization would still be an uncommon route of suppressor generation because suppressor mutations were isolated throughout the length of the protein (Fig. 3E and 4A) rather than near a single motif.

Therefore, we hypothesized that mutations that impact the DNA binding of Hrq1-K318A are a more common way to generate suppressors. To test this hypothesis, we attempted to generate recombinant Hrq1-K318,P732S, -K318A,C979Y, and -K318A,A1006P mutant proteins to analyse their ability to bind ssDNA. Unfortunately, despite repeated attempts, we failed to produce useful amounts of the K318A,C979Y and K318A,A1006P proteins. This is likely due to their apparent instability in yeast (Fig. 3C and 3D), which may be exacerbated in a non-native expression host. However, we did succeed to purifying Hrq1-P732S and Hrq1-K318A,P732S proteins (Fig. 5A).

To ensure that these mutants were properly folded and did not form soluble micro-aggregates, we analysed them by mass photometry (Fig. 5B). Wild-type recombinant Hrq1 is known to oligomerize, with the proportion of different oligomers dependent upon the expression host (25,30). Here, mass photometry revealed the existence of monomers, dimers, trimers, and in some cases, tetramers for our wild-type and mutant preparations (Fig. 5B). As typical with baculovirus expression of Hrq1 in insect cells (30), the monomeric form dominated. Importantly, recombinant Hrq1-P732S and Hrq1-K318A,P732S displayed the same mass photometry profiles as wild-type and Hrq1-K318A (Fig. 5B). When these proteins are denatured with heat and SDS, the oligomeric peaks disappear, and only monomeric protein is evident (*e.g.*, Fig. S5).

Having demonstrated that our Hrq1-P732S and Hrq1-K318A,P732S preparations are stably folded, we next assessed their ability to bind ssDNA. We previously reported that Hrq1-K318A can bind to ssDNA but with approximately twofold lower affinity than Hrq1 (32), and that result is recapitulated here with an IR-labelled poly(dT) 30mer ssDNA ($p = 0.0015$) (Fig. 5C). In comparison, recombinant Hrq1-P732S and Hrq1-K318A,P732S ssDNA binding was markedly reduced compared to wild-type Hrq1 and Hrq1-K318A ($p < 0.0001$). To further characterize these mutant proteins, we also tested their ability to unwind DNA.

bioRxiv preprint doi: https://doi.org/10.64898/2026.02.13.705743; this version posted February 15, 2026. The copyright holder for this preprint (which was not certified by peer review) is the author/funder, who has granted bioRxiv a license to display the preprint in perpetuity. It is made available under a CC-BY-NC 4.0 International license.

Unsurprisingly, for proteins that lacked ssDNA binding activity, Hrq1-P732S and Hrq1-K318A,P732S also lacked helicase activity (Fig. 5D). These data are consistent with the hypothesis that knocking out the DNA binding of Hrq1-K318A should relieve its dominant negative activity and phenocopy an Hrq1 null.

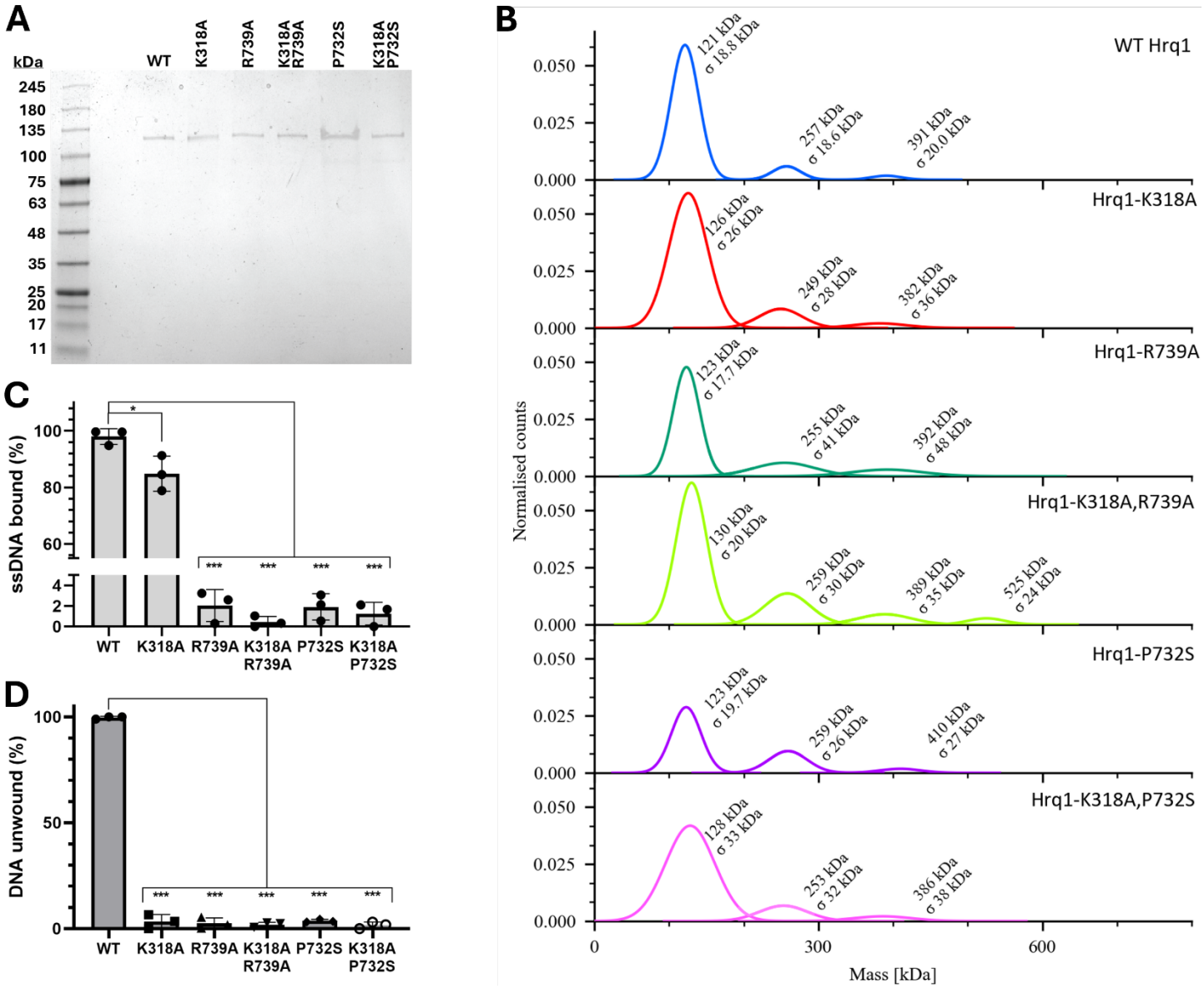


Figure 5. Ablating Hrq1-K318A DNA binding leads to suppression of ICL sensitivity. A) Recombinant wild-type (WT) and single or double-mutant Hrq1 protein preparations. Coomassie-stained SDS-PAGE gel of 2 ng of each of the indicated proteins run alongside a molecular weight marker ladder. **B)** Recombinant wild-type and mutant Hrq1 preparations form multimers in solution. Mass photometry profiles indicate that purified Hrq1 and mutant proteins (~130 kDa) form dimers (~260 kDa), trimers (~390 kDa), and tetramers (~520 kDa). The average molecular weight of single molecules in each Gaussian curve is listed, as well as the standard deviation (σ). **C)** DNA binding activity and **D)** helicase activity of Hrq1 and mutant proteins. Gel shift assays (n = 3) using 200 nM protein and 2 nM ssDNA probe were performed at 30°C to analyse ssDNA binding. Helicase assays used a fork substrate and included ATP to catalyse translocation and unwinding. In both c and D, the individual values are shown for each protein, as well as the average (bars) and standard deviation (error bars). One-way ANOVAs were used to determine significance. *, $p < 0.05$; and ***, $p < 0.001$.

De novo design of a suppressor

bioRxiv preprint doi: https://doi.org/10.64898/2026.02.13.705743; this version posted February 15, 2026. The copyright holder for this preprint (which was not certified by peer review) is the author/funder, who has granted bioRxiv a license to display the preprint in perpetuity. It is made available under a CC-BY-NC 4.0 International license.

As another test of the hypothesis that disrupting the DNA binding activity of Hrq1-K318A is a route of ICL sensitivity suppression, we attempted to design a DNA binding mutant of Hrq1/Hrq1-K318A *de novo*. Assuming that the hypothesis is correct, cells expressing the double mutant with K318A should be resistant to ICL damage. We recently reported that an N-terminal truncation mutant of Hrq1 (Hrq1ΔN) largely lacks ssDNA binding activity (36). Therefore, we combined the ΔN allele with K318A (full-length Hrq1 residue numbering) to create a yeast strain expressing a Hrq1ΔN-K318A mutant and tested it for ICL sensitivity. As previously demonstrated, *hrq1ΔN* cells phenocopy the DEB sensitivity of the *hrq1Δ* strain (Fig. 6A). Here, *hrq1ΔN-K318A* cells behave likewise, being less sensitive to DEB than the *hrq1-K318A* strain and growing more like *hrq1Δ* cells (Fig. 6A). Thus, to a first approximation, inhibiting DNA binding in the Hrq1-K318A mutant does suppress ICL sensitivity. However, recombinant Hrq1ΔN fails to stimulate the Pso2 nuclease *in vitro* (29), likely because the two proteins no longer physically interact. Thus, the comparison of a full-length Hrq1 mutant to this truncation is problematic, especially when considering the Hrq1-Pso2 ICL repair pathway.

To determine if we could rationally design a full-length *hrq1-K318A* second-site suppressor, we turned back to the MrfA enzyme. Several residues in the *B. subtilis* helicase are demonstrated to be involved in ssDNA binding (56), many of which are conserved in *S. cerevisiae* Hrq1. This includes MrfA R491 (R739 in Hrq1; Fig. 6B), which ablates ssDNA binding by MrfA when mutated to an alanine (56). We hypothesized that the R739A mutation in Hrq1 should likewise reduce ssDNA binding. We generated recombinant Hrq1-R739A and Hrq1-K318A,R739A proteins (Fig. 5A) and tested their ssDNA binding activity using gel shifts. Compared to wild-type Hrq1 and Hrq1-K318A, the ability to bind ssDNA by Hrq1-R739A was severely decreased (Fig. 5C and 6C). Similarly, the recombinant Hrq1-K318A, R739A double mutant also lacked DNA binding activity (Fig. 5C).Having proven that the R739A mutation negatively impacts ssDNA binding, we next introduced this mutation into the *hrq1-K318A* locus in yeast and tested the double mutant strain for suppression of DEB sensitivity. As shown in Figure 6D, the *hrq1-K318A,R739A* double mutant is more resistant to DEB damage than *hrq1-K318A*. Compared to the *hrq1Δ* allele, the *hrq1-K318A,R739A* strain is more sensitive, and in that respect phenocopies the intermediate suppression of *hrq1-K318A,P732S* (Fig. 3B and S1). This is perhaps unsurprising given the close proximity of the P732 and R739 residues (Fig. 4A) and their conservation in MrfA (Fig. 6B). However, given that the Hrq1-R739A mutant protein is nearly a ssDNA binding null *in vitro* (Fig. 5C and 6C), the fact that the *hrq1-R739A* single-mutant strain displays nearly wild-type levels of DEB resistance is surprising (Fig. 6D). This phenomenon and others are discussed below.

bioRxiv preprint doi: https://doi.org/10.64898/2026.02.13.705743; this version posted February 15, 2026. The copyright holder for this preprint (which was not certified by peer review) is the author/funder, who has granted bioRxiv a license to display the preprint in perpetuity. It is made available under a CC-BY-NC 4.0 International license.

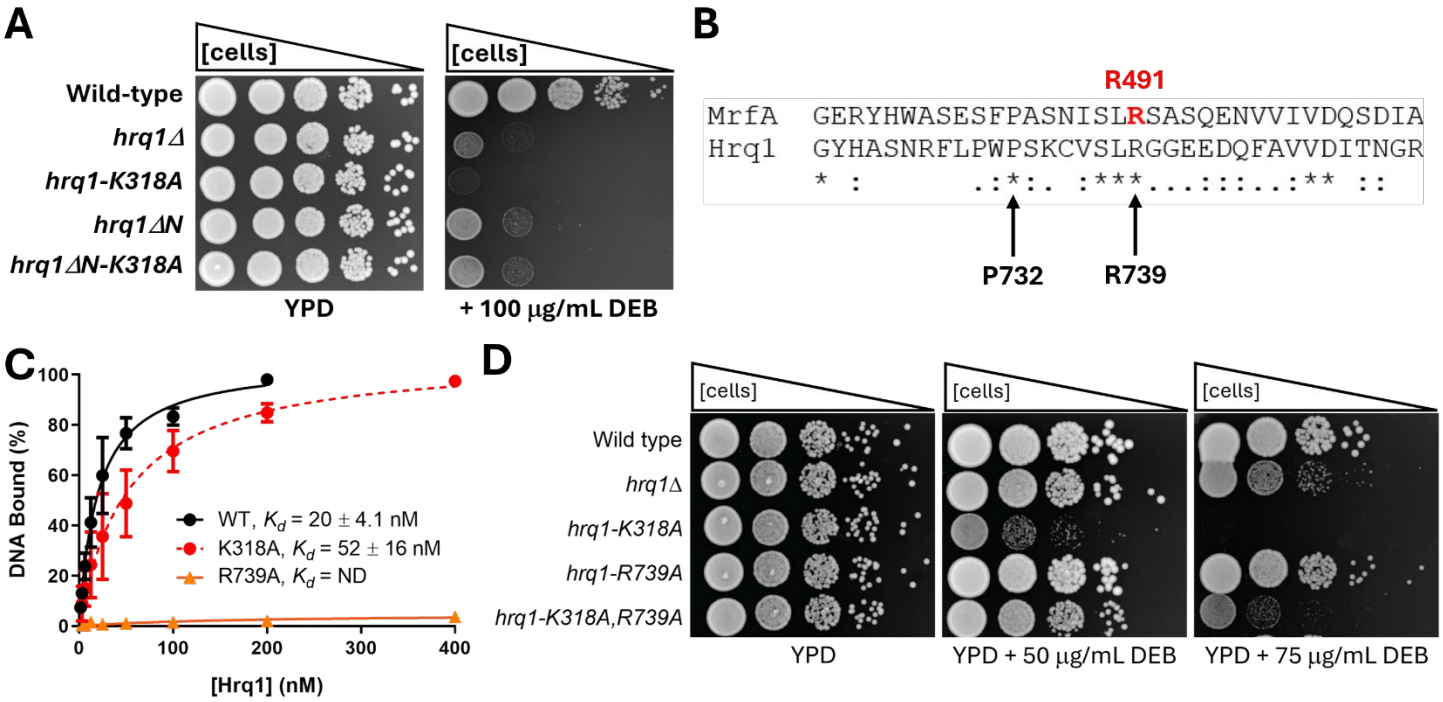


Figure 6. The R739A mutation disrupts Hrq1 ssDNA binding. A) Truncating the N-terminus of Hrq1 suppresses the ICL sensitivity of the K318A mutant. Strains of the indicated genotypes were grown overnight, diluted to OD_{600} = 1, serially diluted tenfold, and then 5 μL of each dilution was spotted on to YPD or YPD supplemented with DEB. **B)** Protein alignment of a conserved peptide in *B. subtilis* MrfA and *S. cerevisiae* Hrq1. MrfA R491 is noted in red, and the Hrq1 P732 and R739 residues are shown. Identical (*), strongly conserved (:), and conserved (.) residues are marked. **C)** Neutralizing R739 negatively impacts Hrq1 ssDNA binding. Gel shift assays (n = 3) using 0-200 or 0-400 nM protein and 2 nM ssDNA probe were performed for the three indicated protein. Binding was quantified, and the averages and standard deviations are plotted. Binding isotherms were fitted to each dataset to calculate the binding affinity (K_d), which could not be determined (ND) for hRq1-R739A due to its poor binding. **D)** The *hrq1-K318A,R739A* mutant is a suppressor of ICL sensitivity. The spot dilution assays were performed as in A using the indicated strains.

DISCUSSION

ICLs pose a severe threat to genome stability by covalently linking the two strands of DNA and blocking replication and transcription (40). In *Saccharomyces cerevisiae*, repair of these lesions relies heavily on the Hrq1 helicase and the Pso2 nuclease, with Hrq1 stimulating Pso2-mediated processing of ICLs (25,28-30,40). In this study, we combined genetic suppressor analysis, structural modeling, and biochemical characterization to investigate the consequences of disabling Hrq1 helicase activity. Our findings demonstrate that the catalytically inactive Hrq1-K318A protein exerts a dominant-negative effect on ICL repair and that this toxicity is relieved primarily by secondary mutations that destabilize Hrq1 or disrupt its ability to bind DNA.

Our initial efforts to identify new ICL repair factors focused on genes transcriptionally upregulated in cells expressing *hrq1-K318A* (34). However, genetic epistasis analysis revealed that *FMP48*, *TDA6*, and *YLR297W* do not measurably contribute to ICL repair, either in the Hrq1–Pso2 pathway or in a proto–Fanconi anemia–like backup pathway (Fig. 1). These results highlight the caution required when inferring functional relevance from transcriptional responses alone, particularly in the context of stress-induced gene expression, and motivated the subsequent use of an unbiased genetic suppressor approach (Fig. 2).

bioRxiv preprint doi: https://doi.org/10.64898/2026.02.13.705743; this version posted February 15, 2026. The copyright holder for this preprint (which was not certified by peer review) is the author/funder, who has granted bioRxiv a license to display the preprint in perpetuity. It is made available under a CC-BY-NC 4.0 International license.

Second-site suppressors in Hrq1-K318A

The spontaneous suppressor screen yielded an unexpected but highly informative result: suppression of *hrq1-K318A* sensitivity to DEB-induced ICL damage occurred overwhelmingly through secondary mutations within the *hrq1-K318A* gene itself. Both whole-genome sequencing and targeted amplicon sequencing demonstrated that the majority of suppressors carried second-site mutations distributed throughout the Hrq1 coding sequence (Fig. 3 and Table 2). Reconstruction of representative mutations confirmed that suppression is monogenic and directly attributable to altered Hrq1 function (Fig. 3B), rather than to the cumulative effects of multiple DEB-induced mutations elsewhere in the genome.

Consistent with previous observations (25,29,30,36), *hrq1-K318A* cells were more sensitive to ICL damage than *hrq1Δ* cells (Fig. 1, 3, 6, and S1), supporting the conclusion that *hrq1-K318A* functions as a dominant-negative allele. This interpretation is further supported by complementation experiments showing that expression of wild-type *HRQ1* efficiently rescued the ICL sensitivity of *hrq1Δ* cells but only weakly alleviated the sensitivity of *hrq1-K318A* cells (Fig. S2). Together, these findings support a model in which Hrq1-K318A is recruited to sites of ICL damage but, lacking ATPase and helicase activity, interferes with or requires a less efficient, alternative repair mechanism that would otherwise partially compensate for complete loss of Hrq1–Pso2 function (Fig. 7). Because Hrq1 and Pso2 likely physically interact during ICL repair (29), Hrq1-K318A may function as a dominant negative simply by binding to Pso2 and restricting it from accessing the lesion.

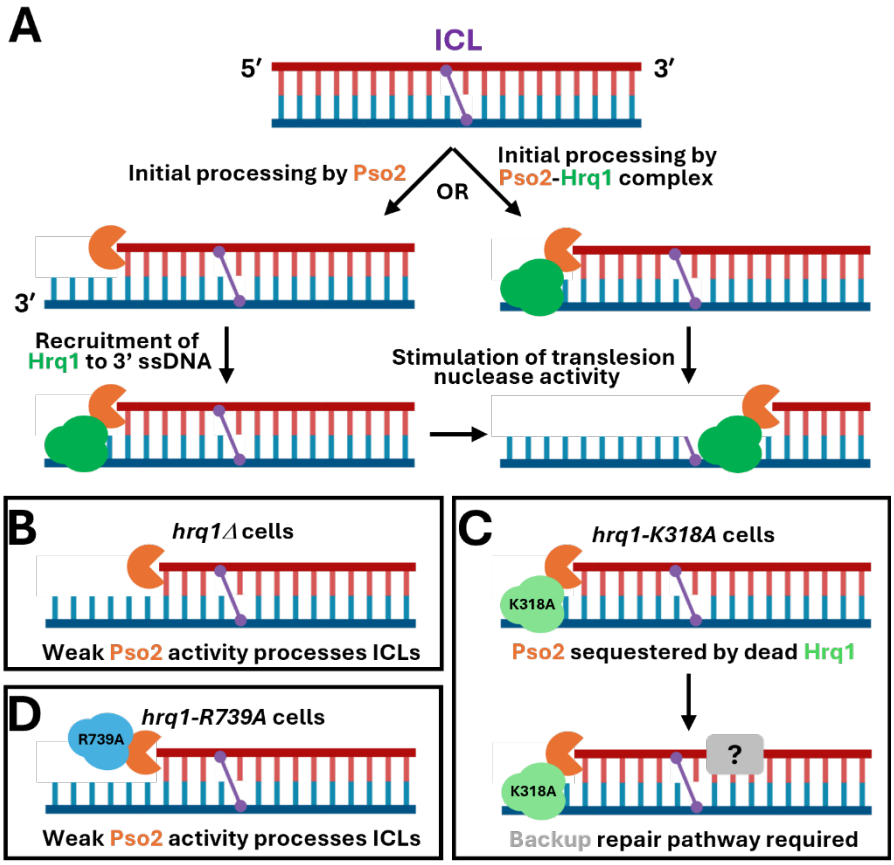


Figure 7. Working model for ICL repair in wild-type and *hrq1* mutant cells. A) When an ICL lesion is formed, Pso2 may initially recognize it or be recruited to it alone to begin degrading one strand of DNA from a 5′ phosphate (left). This would generate a ssDNA substrate for Hrq1 to bind to for 3′-5′ translocation. Alternatively, Hrq1 and Pso2 may be recruited as a single unit for initial processing (right). Both paths lead to stimulation of Pso2 nuclease activity by Hrq1 for ssDNA digestion through the lesion. **B)** In *hrq1Δ* cells, Pso2 is still recruited to repair the ICL but does so weakly in the absence of Hrq1 stimulation. **C)** In *hrq1-K318A* cells, Pso2 association with the non-translocating Hrq1 locks Pso2 in an unproductive state, necessitating compensatory repair mechanisms. Thus, *hrq1-K318A* cells are more sensitive to ICL damage than *hrq1Δ* cells because they largely phenocopy *pso2Δ*. **D)** In *hrq1-R739A* cells or other mutants in which Hrq1 lacks ssDNA binding activity, Hrq1 still binds to Pso2, but Pso2 is not locked down on the DNA and can still process ICLs.

bioRxiv preprint doi: https://doi.org/10.64898/2026.02.13.705743; this version posted February 15, 2026. The copyright holder for this preprint (which was not certified by peer review) is the author/funder, who has granted bioRxiv a license to display the preprint in perpetuity. It is made available under a CC-BY-NC 4.0 International license.

The importance of metal ion coordination by RecQ helicases

Mapping suppressor mutations onto predicted Hrq1 structures revealed no linear mutational hotspots (Fig. 3E) but instead identified clusters in three-dimensional space (Fig. 4A), particularly within the conserved, RecQ4-specific RHCD (27). Several suppressors targeted a conserved $CXCX_3CX_2C$ motif predicted to coordinate a zinc ion (Fig. 4C), analogous to the experimentally validated Zn^{2+}-binding site in the *B. subtilis* homolog MrfA (56,67). Disruption of any residue within this motif suppressed *hrq1-K318A* toxicity (Fig. 4D), most likely by destabilizing the protein, as evidenced by reduced steady-state levels of representative mutants (Fig. 3C) and the inability to over-express and purify homologous mutants in the *M. smegmatis* homolog SftH (65). These findings reinforce the functional importance of this metal-binding motif across RecQ4-family helicases and suggest that its integrity is required for stable DNA engagement. Indeed, human RECQL4 contains a Zn^{2+}-binding site in its RQC domain (68), which may also be required for protein folding and stability.

Importantly, not all suppressors acted by destabilizing Hrq1. For instance, the P732S mutation produced a stable, full-length protein (Fig. 3C) that nonetheless suppressed *hrq1-K318A* sensitivity to ICL damage (Fig. 3A and B). Biochemical analyses revealed that recombinant Hrq1-P732S and Hrq1-K318A,P732S exhibit severely reduced ssDNA binding (Fig. 5C) and helicase activity (Fig. 5D) despite proper folding and oligomerization (Fig. 5B). These results demonstrate that loss of DNA binding alone is sufficient to suppress the *hrq1-K318A* dominant-negative phenotype. This conclusion is further supported by rationally designed suppressors, including the Hrq1ΔN-K318A truncation (Fig. 6A) and the full-length Hrq1-K318A,R739A mutant (Fig. 6B), both of which impair DNA binding (36) and relieve ICL sensitivity to varying degrees (Fig. 6).

Why does the Hrq1-R739A mutation ablate ssDNA binding *in vitro* but support ICL repair *in vivo*?

An apparent discrepancy arises from the behavior of the *hrq1-R739A* single mutant, which displays near–wild-type resistance to DEB-induced ICL damage (Fig. 6D and S1) despite the corresponding recombinant protein exhibiting severely reduced ssDNA binding *in vitro* (Fig 5C and 6C). One explanation is that the ssDNA binding defect observed under defined biochemical conditions may not fully reflect Hrq1 activity in the cellular context. *In vivo*, Hrq1 operates within multiprotein repair assemblies, interacting directly with Pso2 and potentially other factors (25,29,30), which could stabilize DNA engagement or compensate for weakened Hrq1 ssDNA binding. Thus, residual or transient DNA association by Hrq1-R739A may be sufficient to support Hrq1/Pso2–dependent ICL repair in cells.

Alternatively, R739A may preferentially impair binding to isolated ssDNA substrates while preserving interactions with more physiologically relevant DNA structures encountered during ICL repair, such as processed ICL substrates or protein–DNA complexes. Hrq1 recruitment *in vivo* may rely less on high-affinity ssDNA binding and more on cooperative recognition of repair intermediates, an effect that would not be captured by assays using short homopolymeric ssDNA substrates. In this context, the R739A mutation may selectively disrupt nonproductive DNA engagement that underlies the dominant-negative activity of Hrq1-K318A, while leaving productive repair-associated interactions largely intact.

bioRxiv preprint doi: https://doi.org/10.64898/2026.02.13.705743; this version posted February 15, 2026. The copyright holder for this preprint (which was not certified by peer review) is the author/funder, who has granted bioRxiv a license to display the preprint in perpetuity. It is made available under a CC-BY-NC 4.0 International license.

A further possibility is that Hrq1-R739A retains sufficient helicase-independent scaffolding function to support ICL repair. Hrq1 has been proposed to act not only as an enzyme but also as a structural component that organizes repair factors at sites of damage (25,29,30,32,34,35,61). Weakening ssDNA binding may diminish the residence time of Hrq1 on DNA without abolishing its ability to transiently interact with partner proteins, thereby avoiding dominant-negative interference while still permitting repair. Consistent with this idea, combining R739A with the K318A mutation suppresses ICL sensitivity (Fig. 6D and S1), suggesting that the primary liability of Hrq1-K318A lies in persistent, nonproductive DNA engagement rather than in loss of Hrq1-dependent scaffolding *per se*.

Together, these observations highlight an important distinction between DNA binding as measured *in vitro* and the functional requirements for Hrq1 activity *in vivo*. They further reinforce the conclusion that dominant-negative toxicity arises from stable DNA association by a catalytically inactive helicase, whereas partial or weakened DNA binding can be compatible with effective ICL repair.

Working model for ICL repair in yeast

Collectively, these findings support a model in which DNA binding without catalytic activity converts Hrq1 into a toxic roadblock during ICL repair (Fig. 7). In this model, Hrq1-K318A is recruited to ICL-associated DNA structures but cannot translocate or remodel the substrate, thereby blocking access by compensatory repair enzymes or requiring non-optimal backup repair mechanisms (Fig. 7B). Secondary mutations that destabilize Hrq1 or prevent its association with DNA alleviate this blockade, allowing alternative repair pathways to function and restoring resistance to ICL damage (Fig. 7C). This framework explains why *hrq1-K318A* mutants are more deleterious than *hrq1Δ* mutants and why suppression can be achieved through a wide variety of intragenic second-site mutations.

Although our study is focused on *S. cerevisiae* Hrq1, the mechanistic principles described here are likely relevant to RecQ4-family helicases more broadly. Human RECQL4 plays essential roles in genome maintenance, and pathogenic RECQ4 variants may retain partial expression or DNA binding capacity while exhibiting reduced catalytic activity (18,21,23,26,38,69-75). Our findings suggest that such alleles may be deleterious not simply because of loss of helicase function, but because persistent DNA binding by catalytically impaired proteins can actively interfere with repair processes. By separating the contributions of DNA binding and enzymatic activity, this work provides a conceptual framework for understanding how incomplete loss-of-function mutations in RecQ4-family helicases may have more severe consequences than null alleles. It also suggests that using small molecules to target DNA binding by catalytically inactive disease alleles of human RECQL4 is a viable treatment strategy to mitigate the pathogenic effects if the helicase mutation.

In summary, this study reveals DNA binding as the central determinant of dominant-negative Hrq1 activity during ICL repair and demonstrates that disrupting this interaction suppresses repair defects caused by catalytic inactivation. These findings refine our understanding of Hrq1 function, illuminate the hazards of helicase engagement without catalysis, and provide mechanistic insight into how RecQ4-family helicases contribute to genome stability.

bioRxiv preprint doi: https://doi.org/10.64898/2026.02.13.705743; this version posted February 15, 2026. The copyright holder for this preprint (which was not certified by peer review) is the author/funder, who has granted bioRxiv a license to display the preprint in perpetuity. It is made available under a CC-BY-NC 4.0 International license.

DATA AVAILABILITY

The data underlying this article are available in the article, in its online supplementary material, or will be shared upon reasonable request to the corresponding author.

SUPPLEMENTARY DATA

Supplementary Data are available at NAR online.

ACKNOWLEDGEMENTS

We thank members of the Bochman lab for providing insightful feedback during the course of this work. We wish to acknowledge and honor the myaamiaki, Lënape, Bodwéwadmik, and saawanwa people, on whose ancestral homelands and resources Indiana University Bloomington is built.

AUTHOR CONTRIBUTIONS

Robert Simmons: Conceptualization, Formal analysis, Methodology, Validation, Writing—original draft. Faith E. McDevitt: Formal analysis, Methodology, Validation, Writing— review & editing. Alexandra Hurlock: Formal analysis, Methodology, Validation, Writing— review & editing. Michael E. Kumcu: Formal analysis, Methodology, Validation, Writing— review & editing. Matthew Bochman: Conceptualization, Formal analysis, Methodology, Validation, Writing— review & editing.

FUNDING

This work was supported by the National Institutes of Health [R35GM133437] and start-up funds from Indiana University to M.L.B.

CONFLICT OF INTEREST DISCLOSURE

The authors declare no conflicts of interest.

bioRxiv preprint doi: https://doi.org/10.64898/2026.02.13.705743; this version posted February 15, 2026. The copyright holder for this preprint (which was not certified by peer review) is the author/funder, who has granted bioRxiv a license to display the preprint in perpetuity. It is made available under a CC-BY-NC 4.0 International license.

REFERENCES

1. Croteau, D.L., Popuri, V., Opresko, P.L. and Bohr, V.A. (2014) Human RecQ helicases in DNA repair, recombination, and replication. *Annu Rev Biochem*, **83**, 519-552.
2. Abu-Libdeh, B., Jhujh, S.S., Dhar, S., Sommers, J.A., Datta, A., Longo, G.M., Grange, L.J., Reynolds, J.J., Cooke, S.L., McNee, G.S. *et al.* (2022) RECON syndrome is a genome instability disorder caused by mutations in the DNA helicase RECQL1. *J Clin Invest*, **132**.
3. Larizza, L., Roversi, G. and Volpi, L. (2010) Rothmund-Thomson syndrome. *Orphanet J Rare Dis*, **5**, 2.
4. Lee, J.W., Harrigan, J., Opresko, P.L. and Bohr, V.A. (2005) Pathways and functions of the Werner syndrome protein. *Mech. Ageing Dev.*, **126**, 79-86.
5. Langer, K., Cunniff, C.M. and Kucine, N. (1993) In Adam, M. P., Bick, S., Mirzaa, G. M., Pagon, R. A., Wallace, S. E. and Amemiya, A. (eds.), *GeneReviews((R))*, Seattle (WA).
6. Mojumdar, A. (2020) Mutations in conserved functional domains of human RecQ helicases are associated with diseases and cancer: A review. *Biophys Chem*, **265**, 106433.
7. Gupta, P., Majumdar, A.G. and Patro, B.S. (2022) Enigmatic role of WRN-RECQL helicase in DNA repair and its implications in cancer. *J Transl Genet Genom*, **6**, 147-156.
8. Baltgalvis, K.A., Lamb, K.N., Symons, K.T., Wu, C.C., Hoffman, M.A., Snead, A.N., Song, X., Glaza, T., Kikuchi, S., Green, J.C. *et al.* (2024) Chemoproteomic discovery of a covalent allosteric inhibitor of WRN helicase. *Nature*, **629**, 435-442.
9. Ferretti, S., Hamon, J., de Kanter, R., Scheufler, C., Andraos-Rey, R., Barbe, S., Bechter, E., Blank, J., Bordas, V., Dammassa, E. *et al.* (2024) Discovery of WRN inhibitor HRO761 with synthetic lethality in MSI cancers. *Nature*, **629**, 443-449.
10. van Wietmarschen, N., Sridharan, S., Nathan, W.J., Tubbs, A., Chan, E.M., Callen, E., Wu, W., Belinky, F., Tripathi, V., Wong, N. *et al.* (2020) Repeat expansions confer WRN dependence in microsatellite-unstable cancers. *Nature*, **586**, 292-298.
11. Behan, F.M., Iorio, F., Picco, G., Goncalves, E., Beaver, C.M., Migliardi, G., Santos, R., Rao, Y., Sassi, F., Pinnelli, M. *et al.* (2019) Prioritization of cancer therapeutic targets using CRISPR-Cas9 screens. *Nature*, **568**, 511-516.
12. Chan, E.M., Shibue, T., McFarland, J.M., Gaeta, B., Ghandi, M., Dumont, N., Gonzalez, A., McPartlan, J.S., Li, T., Zhang, Y. *et al.* (2019) WRN helicase is a synthetic lethal target in microsatellite unstable cancers. *Nature*, **568**, 551-556.
13. Chen, J., Situ, Y., Cai, J., Liao, W.Y., Jiang, D.B., Huang, C.S., Zheng, J.C., Peng, L.J. and Lin, H. (2026) Upregulated BLM and RECQL4 in Osteosarcoma: Association with Poor Prognosis, Immune Cell Infiltration, and Inhibitory Effects of Sphingosine Kinase 1 Inhibitor II/Pilaralisib. *Immunotargets Ther*, **15**.
14. Ma, X., Tian, F., Xiao, Y., Huang, M., Song, D., Chen, X. and Xu, H. (2024) Synergistic effects of bloom helicase (BLM) inhibitor AO/854 with cisplatin in prostate cancer. *Sci Rep*, **14**, 24962.
15. Ovejero, S., Viziteu, E., Dutrieux, L., Devin, J., Lin, Y.L., Alaterre, E., Jourdan, M., Basbous, J., Requirand, G., Robert, N. *et al.* (2022) The BLM helicase is a new therapeutic target in multiple myeloma involved in replication stress survival and drug resistance. *Front Immunol*, **13**, 983181.
16. Ma, X.Y., Xu, H.Q., Zhao, J.F., Ruan, Y. and Chen, B. (2022) Discovery of a Novel Bloom's Syndrome Protein (BLM) Inhibitor Suppressing Growth and Metastasis of Prostate Cancer. *Int J Mol Sci*, **23**.
17. Kaczmarczyk, A., Sokolowski, M., Wojnicki, K., Pabis, M., Wojtas, B., Ciechomska, I.A., Poleszak, K., Gielniewski, B., Krol, S.K., Guille, M. *et al.* (2025) Novel mutations in the RECQL4 gene affect its helicase functions, interactions with the BLM helicase and chemotherapeutics-induced cell death. *Cell Death Discov*, **11**, 560.

bioRxiv preprint doi: https://doi.org/10.64898/2026.02.13.705743; this version posted February 15, 2026. The copyright holder for this preprint (which was not certified by peer review) is the author/funder, who has granted bioRxiv a license to display the preprint in perpetuity. It is made available under a CC-BY-NC 4.0 International license.

18. Balajee, A.S. (2021) Human RecQL4 as a Novel Molecular Target for Cancer Therapy. *Cytogenet Genome Res*, **161**, 305-327.
19. Yokoyama, H., Moreno-Andres, D., Astrinidis, S.A., Hao, Y., Weberruss, M., Schellhaus, A.K., Lue, H., Haramoto, Y., Gruss, O.J. and Antonin, W. (2019) Chromosome alignment maintenance requires the MAP RECQL4, mutated in the Rothmund-Thomson syndrome. *Life Sci Alliance*, **2**.
20. Singh, D.K., Popuri, V., Kulikowicz, T., Shevelev, I., Ghosh, A.K., Ramamoorthy, M., Rossi, M.L., Janscak, P., Croteau, D.L. and Bohr, V.A. (2012) The human RecQ helicases BLM and RECQL4 cooperate to preserve genome stability. *Nucleic Acids Res*, **40**, 6632-6648.
21. Su, Y., Meador, J.A., Calaf, G.M., Proietti De-Santis, L., Zhao, Y., Bohr, V.A. and Balajee, A.S. (2010) Human RecQL4 helicase plays critical roles in prostate carcinogenesis. *Cancer Res*, **70**, 9207-9217.
22. Kamimura, Y., Masumoto, H., Sugino, A. and Araki, H. (1998) Sld2, which interacts with Dpb11 in Saccharomyces cerevisiae, is required for chromosomal DNA replication. *Mol Cell Biol*, **18**, 6102-6109.
23. Xu, X., Chang, C.W., Li, M., Liu, C. and Liu, Y. (2021) Molecular Mechanisms of the RECQ4 Pathogenic Mutations. *Front Mol Biosci*, **8**, 791194.
24. Abe, T., Yoshimura, A., Hosono, Y., Tada, S., Seki, M. and Enomoto, T. (2011) The N-terminal region of RECQL4 lacking the helicase domain is both essential and sufficient for the viability of vertebrate cells. Role of the N-terminal region of RECQL4 in cells. *Biochim Biophys Acta*, **1813**, 473-479.
25. Bochman, M.L., Paeschke, K., Chan, A. and Zakian, V.A. (2014) Hrq1, a homolog of the human RecQ4 helicase, acts catalytically and structurally to promote genome integrity. *Cell Rep*, **6**, 346-356.
26. Macris, M.A., Krejci, L., Bussen, W., Shimamoto, A. and Sung, P. (2006) Biochemical characterization of the RECQ4 protein, mutated in Rothmund-Thomson syndrome. *DNA Repair (Amst)*, **5**, 172-180.
27. Barea, F., Tessaro, S. and Bonatto, D. (2008) In silico analyses of a new group of fungal and plant RecQ4-homologous proteins. *Comput Biol Chem*, **32**, 349-358.
28. Rogers, C.M. and Bochman, M.L. (2017) Saccharomyces cerevisiae Hrq1 helicase activity is affected by the sequence but not the length of single-stranded DNA. *Biochem Biophys Res Commun*, **486**, 1116-1121.
29. Rogers, C.M., Lee, C.Y., Parkins, S., Buehler, N.J., Wenzel, S., Martinez-Marquez, F., Takagi, Y., Myong, S. and Bochman, M.L. (2020) The yeast Hrq1 helicase stimulates Pso2 translesion nuclease activity and thereby promotes DNA interstrand crosslink repair. *J Biol Chem*, **295**, 8945-8957.
30. Rogers, C.M., Wang, J.C., Noguchi, H., Imasaki, T., Takagi, Y. and Bochman, M.L. (2017) Yeast Hrq1 shares structural and functional homology with the disease-linked human RecQ4 helicase. *Nucleic Acids Res*, **45**, 5217-5230.
31. Nickens, D.G. and Bochman, M.L. (2022) Genetic and biochemical interactions of yeast DNA helicases. *Methods*, **204**, 234-240.
32. Nickens, D.G., Rogers, C.M. and Bochman, M.L. (2018) The Saccharomyces cerevisiae Hrq1 and Pif1 DNA helicases synergistically modulate telomerase activity in vitro. *J Biol Chem*, **293**, 14481-14496.
33. Nickens, D.G., Sausen, C.W. and Bochman, M.L. (2019) The Biochemical Activities of the Saccharomyces cerevisiae Pif1 Helicase Are Regulated by Its N-Terminal Domain. *Genes (Basel)*, **10**.

bioRxiv preprint doi: https://doi.org/10.64898/2026.02.13.705743; this version posted February 15, 2026. The copyright holder for this preprint (which was not certified by peer review) is the author/funder, who has granted bioRxiv a license to display the preprint in perpetuity. It is made available under a CC-BY-NC 4.0 International license.

34. Rogers, C.M., Sanders, E., Nguyen, P.A., Smith-Kinnaman, W., Mosley, A.L. and Bochman, M.L. (2020) The Genetic and Physical Interactomes of the Saccharomyces cerevisiae Hrq1 Helicase. *G3 (Bethesda)*, **10**, 4347-4357.
35. Sanders, E., Nguyen, P.A., Rogers, C.M. and Bochman, M.L. (2020) Comprehensive Synthetic Genetic Array Analysis of Alleles That Interact with Mutation of the Saccharomyces cerevisiae RecQ Helicases Hrq1 and Sgs1. *G3 (Bethesda)*, **10**, 4359-4368.
36. Shumaker, K.A., Kumcu, M.E., McDevitt, F.E., Rogers, C.M. and Bochman, M.L. (2025) A screen for synthetic genetic interactions with the Saccharomyces cerevisiae hrq1DeltaN allele. *G3 (Bethesda)*.
37. Luong, T.T., Li, Z., Priedigkeit, N., Parker, P.S., Bohm, S., Rapchak, K., Lee, A.V. and Bernstein, K.A. (2022) Hrq1/RECQL4 regulation is critical for preventing aberrant recombination during DNA intrastrand crosslink repair and is upregulated in breast cancer. *PLoS Genet*, **18**, e1010122.
38. Jin, W., Liu, H., Zhang, Y., Otta, S.K., Plon, S.E. and Wang, L.L. (2008) Sensitivity of RECQL4-deficient fibroblasts from Rothmund-Thomson syndrome patients to genotoxic agents. *Hum Genet*, **123**, 643-653.
39. Mo, D., Fang, H., Niu, K., Liu, J., Wu, M., Li, S., Zhu, T., Aleskandarany, M.A., Arora, A., Lobo, D.N. *et al.* (2016) Human Helicase RECQL4 Drives Cisplatin Resistance in Gastric Cancer by Activating an AKT-YB1-MDR1 Signaling Pathway. *Cancer Res*, **76**, 3057-3066.
40. Rogers, C.M., Simmons III, R.H., Fluhler Thornburg, G.E., Buehler, N.J. and Bochman, M.L. (2020) Fanconi anemia-independent DNA inter-strand crosslink repair in eukaryotes. *Prog Biophys Mol Biol*.
41. Herskowitz, I. (1987) Functional inactivation of genes by dominant negative mutations. *Nature*, **329**, 219-222.
42. Veitia, R.A. (2007) Exploring the molecular etiology of dominant-negative mutations. *Plant Cell*, **19**, 3843-3851.
43. Meeks-Wagner, D. and Hartwell, L.H. (1986) Normal stoichiometry of histone dimer sets is necessary for high fidelity of mitotic chromosome transmission. *Cell*, **44**, 43-52.
44. Lagna, G. and Hemmati-Brivanlou, A. (1998) Use of dominant negative constructs to modulate gene expression. *Curr Top Dev Biol*, **36**, 75-98.
45. Stark, J.M., Hu, P., Pierce, A.J., Moynahan, M.E., Ellis, N. and Jasin, M. (2002) ATP hydrolysis by mammalian RAD51 has a key role during homology-directed DNA repair. *J Biol Chem*, **277**, 20185-20194.
46. Pellegrini, L., Yu, D.S., Lo, T., Anand, S., Lee, M., Blundell, T.L. and Venkitaraman, A.R. (2002) Insights into DNA recombination from the structure of a RAD51-BRCA2 complex. *Nature*, **420**, 287-293.
47. Wang, A.T., Kim, T., Wagner, J.E., Conti, B.A., Lach, F.P., Huang, A.L., Molina, H., Sanborn, E.M., Zierhut, H., Cornes, B.K. *et al.* (2015) A Dominant Mutation in Human RAD51 Reveals Its Function in DNA Interstrand Crosslink Repair Independent of Homologous Recombination. *Mol Cell*, **59**, 478-490.
48. So, A., Dardillac, E., Muhammad, A., Chailleux, C., Sesma-Sanz, L., Ragu, S., Le Cam, E., Canitrot, Y., Masson, J.Y., Dupaigne, P. *et al.* (2022) RAD51 protects against nonconservative DNA double-strand break repair through a nonenzymatic function. *Nucleic Acids Res*, **50**, 2651-2666.
49. George, J.W., Brosh, R.M., Jr. and Matson, S.W. (1994) A dominant negative allele of the Escherichia coli uvrD gene encoding DNA helicase II. A biochemical and genetic characterization. *J Mol Biol*, **235**, 424-435.

bioRxiv preprint doi: https://doi.org/10.64898/2026.02.13.705743; this version posted February 15, 2026. The copyright holder for this preprint (which was not certified by peer review) is the author/funder, who has granted bioRxiv a license to display the preprint in perpetuity. It is made available under a CC-BY-NC 4.0 International license.

50. Taneja, P., Gu, J., Peng, R., Carrick, R., Uchiumi, F., Ott, R.D., Gustafson, E., Podust, V.N. and Fanning, E. (2002) A dominant-negative mutant of human DNA helicase B blocks the onset of chromosomal DNA replication. *J Biol Chem*, **277**, 40853-40861.
51. Wu, Y. and Brosh, R.M., Jr. (2010) Helicase-inactivating mutations as a basis for dominant negative phenotypes. *Cell Cycle*, **9**, 4080-4090.
52. Sikorski, R.S. and Hieter, P. (1989) A system of shuttle vectors and yeast host strains designed for efficient manipulation of DNA in *Saccharomyces cerevisiae*. *Genetics*, **122**, 19-27.
53. Longtine, M.S., McKenzie, A., 3rd, Demarini, D.J., Shah, N.G., Wach, A., Brachat, A., Philippsen, P. and Pringle, J.R. (1998) Additional modules for versatile and economical PCR-based gene deletion and modification in *Saccharomyces cerevisiae*. *Yeast*, **14**, 953-961.
54. Larkin, M.A., Blackshields, G., Brown, N.P., Chenna, R., McGettigan, P.A., McWilliam, H., Valentin, F., Wallace, I.M., Wilm, A., Lopez, R. *et al.* (2007) Clustal W and Clustal X version 2.0. *Bioinformatics*, **23**, 2947-2948.
55. von der Haar, T. (2007) Optimized protein extraction for quantitative proteomics of yeasts. *PLoS One*, **2**, e1078.
56. Roske, J.J., Liu, S., Loll, B., Neu, U. and Wahl, M.C. (2021) A skipping rope translocation mechanism in a widespread family of DNA repair helicases. *Nucleic Acids Res*, **49**, 504-518.
57. Neuhoff, V., Arold, N., Taube, D. and Ehrhardt, W. (1988) Improved staining of proteins in polyacrylamide gels including isoelectric focusing gels with clear background at nanogram sensitivity using Coomassie Brilliant Blue G-250 and R-250. *Electrophoresis*, **9**, 255-262.
58. Kang, D.H., Gho, Y.S., Suh, M.K. and Kang, C.H. (2002) Highly sensitive and fast protein detection with coomassie brilliant blue in sodium dodecyl sulfate-polyacrylamide gel electrophoresis. *B Korean Chem Soc*, **23**, 1511-1512.
59. Nickens, D.G., Feng, Z., Shen, J., Gray, S.J., Simmons, R.H., 3rd, Niu, H. and Bochman, M.L. (2024) Cdc13 exhibits dynamic DNA strand exchange in the presence of telomeric DNA. *Nucleic Acids Res*, **52**, 6317-6332.
60. Nickens, D.G., Gray, S.J., Simmons, R.H., 3rd and Bochman, M.L. (2025) Dimerization of Cdc13 is essential for dynamic DNA exchange on telomeric DNA. *J Biol Chem*, **301**, 110496.
61. Simmons, R.H., 3rd, Rogers, C.M. and Bochman, M.L. (2021) A deep dive into the RecQ interactome: something old and something new. *Curr Genet*, **67**, 761-767.
62. Fusco, D., Gralka, M., Kayser, J., Anderson, A. and Hallatschek, O. (2016) Excess of mutational jackpot events in expanding populations revealed by spatial Luria-Delbruck experiments. *Nat Commun*, **7**, 12760.
63. Ellison, M.A., Walker, J.L., Ropp, P.J., Durrant, J.D. and Arndt, K.M. (2020) MutantHuntWGS: A Pipeline for Identifying Saccharomyces cerevisiae Mutations. *G3 (Bethesda)*, **10**, 3009-3014.
64. Bochman, M.L. (2014) Roles of DNA helicases in the maintenance of genome integrity. *Mol Cell Oncol*, **1**, e963429.
65. Yakovleva, L. and Shuman, S. (2012) Mycobacterium smegmatis SftH exemplifies a distinctive clade of superfamily II DNA-dependent ATPases with 3' to 5' translocase and helicase activities. *Nucleic Acids Res*, **40**, 7465-7475.
66. Kosugi, S., Hasebe, M., Tomita, M. and Yanagawa, H. (2009) Systematic identification of cell cycle-dependent yeast nucleocytoplasmic shuttling proteins by prediction of composite motifs. *Proc Natl Acad Sci*, **106**, 10171-10176.
67. Burby, P.E. and Simmons, L.A. (2019) A bacterial DNA repair pathway specific to a natural antibiotic. *Mol Microbiol*, **111**, 338-353.
68. Kaiser, S., Sauer, F. and Kisker, C. (2017) The structural and functional characterization of human RecQ4 reveals insights into its helicase mechanism. *Nat Commun*, **8**, 15907.

bioRxiv preprint doi: https://doi.org/10.64898/2026.02.13.705743; this version posted February 15, 2026. The copyright holder for this preprint (which was not certified by peer review) is the author/funder, who has granted bioRxiv a license to display the preprint in perpetuity. It is made available under a CC-BY-NC 4.0 International license.

69. Liu, Y. (2010) Rothmund-Thomson syndrome helicase, RECQ4: On the crossroad between DNA replication and repair. *DNA Repair (Amst)*, **9**, 325-330.
70. Xu, X. and Liu, Y. (2009) Dual DNA unwinding activities of the Rothmund-Thomson syndrome protein, RECQ4. *Embo J*, **28**, 568-577.
71. Fang, H., Nie, L., Chi, Z., Liu, J., Guo, D., Lu, X., Hei, T.K., Balajee, A.S. and Zhao, Y. (2013) RecQL4 helicase amplification is involved in human breast tumorigenesis. *PLoS One*, **8**, e69600.
72. Ho, S.K.L., Tong, G.P.Y., Leung, L.T., Cheng, S.S.W., Fu, E.C.H., Lo, I.F.M., Liu, A.P.Y. and Luk, H.M. (2025) RECQL4-related Rothmund-Thomson syndrome: A case series and literature review. *Cancer Genet*, **292-293**, 131-136.
73. Li, J., Jin, J., Liao, M., Dang, W., Chen, X., Wu, Y. and Liao, W. (2018) Upregulation of RECQL4 expression predicts poor prognosis in hepatocellular carcinoma. *Oncol Lett*, **15**, 4248-4254.
74. Mo, D., Zhao, Y. and Balajee, A.S. (2018) Human RecQL4 helicase plays multifaceted roles in the genomic stability of normal and cancer cells. *Cancer Lett*, **413**, 1-10.
75. Siitonen, H.A., Sotkasiira, J., Biervliet, M., Benmansour, A., Capri, Y., Cormier-Daire, V., Crandall, B., Hannula-Jouppi, K., Hennekam, R., Herzog, D. *et al.* (2009) The mutation spectrum in RECQL4 diseases. *Eur J Hum Genet*, **17**, 151-158.